

Non-locality and Intermittency in 3D Turbulence

J-P. Laval¹, B. Dubrulle^{2,3}, and S. Nazarenko⁴

October 22, 2018

¹ IGPP, UCLA, 3845 Slichter Hall, Los Angeles, CA 90095, USA

² CE Saclay, F-91190 Gif sur Yvette Cedex, France

³ CNRS, UMR 5572, Observatoire Midi-Pyrénées, 14 avenue Belin, F-31400 Toulouse, France

⁴ Mathematics Institute University of Warwick COVENTRY CV4 7AL, UK

Abstract

Numerical simulations are used to determine the influence of the non-local and local interactions on the intermittency corrections in the scaling properties of 3D turbulence. We show that neglect of local interactions leads to an enhanced small-scale energy spectrum and to a significantly larger number of very intense vortices (“tornadoes”) and stronger intermittency (e.g. wider tails in the probability distribution functions of velocity increments and greater anomalous corrections). On the other hand, neglect of the non-local interactions results in even stronger small-scale spectrum but significantly weaker intermittency. Thus, the amount of intermittency is not determined just by the mean intensity of the small scales, but it is non-trivially shaped by the nature of the scale interactions. Namely, the role of the non-local interactions is to generate intense vortices responsible for intermittency and the role of the local interactions is to dissipate

them. Based on these observations, a new model of turbulence is proposed, in which non-local (RDT-like) interactions couple large and small scale via a multiplicative process with additive noise and the local interactions are modeled by a turbulent viscosity. This model is used to derive a simple toy version of the Langevin equations for small-scale velocity increments. A Gaussian approximation for the large scale fields yields the Fokker-Planck equation for the probability distribution function of the velocity increments. Steady state solutions of this equation allows to qualitatively explain the anomalous corrections and the skewness generation along scale. A crucial role is played by the correlation between the additive and the multiplicative (large-scale) process, featuring the correlation between the stretching and the vorticity.

A puzzling feature of three-dimensional turbulence are the large deviations from Gaussianity observed as one probes smaller and smaller scales. These deviations are usually believed to be associated with the spatial intermittency of small-scale structures, organized into very thin and elongated intense vortices (“tornadoes”)[44, 49, 43]. They are responsible for anomalous corrections to the normal scaling behavior of structure functions associated with the Kolmogorov 1941 [25] picture of turbulence. In this picture, energy containing structures (the so-called ”eddies”) at a given scale, interact with other eddies of smaller but comparable size to transfer energy at a constant rate down to the dissipative scale. A simple prediction of this local picture of turbulence is the famous $k^{-5/3}$ energy spectrum, which has been observed in numerous high Reynolds number experimental data and numerical simulations. The local theory of turbulence further leads to the prediction that the n^{th} moment of a velocity increment $\delta u_\ell = u(x + \ell) - u(x)$ over a distance ℓ should scale like $\ell^{n/3}$. This behavior has never been observed in turbulent flows, and is it now widely admitted that anomalous corrections exist at any finite Reynolds number. Various scenarii have been so far proposed to explain and compute the anomalous corrections. To mention but a few: spatial intermittency of the energy dissipation [26], multi-fractal scaling [40], large deviations of multiplicative cascades [21], extremum principle [11], zero-modes of differential operators [22], scale covariance [15] . These approaches all try to model the breakdown of the exact local scale invariance underlying the Kolmogorov 1941 picture. In a recent study of finite size effects, Dubrulle [17] showed that some properties of the structure functions (non-power law behavior, nonlinear exponents,..) could be explained within a framework in which finite size cut-offs play a central role, and are felt throughout the so-called ”inertial range”. Such finding is in clear contradiction with the ”local” K41 theory, in which eddies in the inertial range are insensitive to the UV and IR end of the energy spectrum, and only interact with their neighbors (in the scale space) via ”local” interactions (involving triads of comparable size). This observation motivated us to consider a new scenario for turbulence, in which anomalous corrections and deviations from Gaussianity are the result of *non-local interactions* between energy containing structures. By non-local interactions, we mean interactions between well separated scales (or highly elongated wavenumber triads). A numerical analysis on the role of the different triadic interactions in the energy cascade have been previously done by Brasseur et al [7] and Domaradzki et al [13]. We have recently demon-

strated via high resolution numerical simulations that in 2D turbulence, the small scale dynamics is essentially governed by their non-local interactions with the large scales [30], [31]. This feature seems natural in view of the large-scale condensation of vortices [6]. As a result, the weak small scales are more influenced by the strong large-scale advection and shearing, than by mutual interactions between themselves. This makes non-local interactions the dominant process at small scales.

2D turbulence is very special, because there is no vortex stretching. As a result, there is no increase of vorticity towards smaller scales as is observed in 3D turbulence. A quantitative feature underlying this difference is the shape of the energy spectra at small scales: it is k^{-3} in 2D turbulence, much steeper than $k^{-5/3}$ 3D energy spectra. In fact, a simple estimate shows that the borderline between local and non-local behaviors is precisely this k^{-3} spectrum: only for energy spectra steeper than k^{-3} can one prove rigorously that the dominant interactions are non-local. It is therefore not our intention to claim that 3D turbulence is non-local, and in fact we do believe that local interactions are responsible for the $k^{-5/3}$ energy spectra. However, it is not unreasonable to think that evolution of the higher cumulants (responsible for deviations from Gaussianity at large deviations) is more non-local than it is for the energy spectrum. Indeed, calculation of higher cumulants in Fourier space involves integrations over larger sets of wavenumbers which (even if close in values pairwise) cover larger range of scales than in the case of lower order cumulants.

A natural tool to study the role of the non-local interactions is the numerical simulation, because it allows a direct check of their influence by artificial switching-off of the elongated wavenumber triads in the Navier-Stokes equations or, on the contrary, retaining only such triads. A limitation of this approach lies in the restricted range of Reynolds number we are able to simulate. However, a recent comparison [3] showed that anomalous corrections and intermittency effects are quite insensitive to the Reynolds number. This shows relevance of a low Reynolds number numerical study of intermittency. This approach is detailed in the next section, where we examine the dynamical role of the local interactions at the small scales using a simulation in which these interactions have been removed. We show that, as compared with a full simulation of the Navier-Stokes equations, such “nonlocal” simulation exhibits a flatter spectrum at small scales and stronger intermittency. As a qualitative indicator of intermittency we use plots of the vortex struc-

tures whose intensity greatly exceeds the r.m.s. vorticity value (“tornadoes”) and PDF’s plots, whereas to quantify intermittency we measure the structure function scaling exponents. We show that main effect of the local interactions can be approximately described by a turbulent viscosity, while the non-local interactions are responsible for development of the localized intense vortices and the deviations of Gaussianity. To validate that the enhanced intermittency is not merely a result of the increased mean small-scale intensity (which could be also caused by some reason other than the non-locality) we perform another numerical experiment in which the elongated triads were removed. Such “local” experiment resulted in even stronger small-scale intensity but the intermittency became clearly weaker. In the Section 2, we show how our findings can be used to provide both a qualitative estimate of the intermittency exponents, and a derivation of the Langevin equations for the velocity increments.

1 Non-local interactions in 3D turbulence

1.1 The problematics

We consider the Navier-Stokes equations:

$$\partial_t \mathbf{u} + \mathbf{u} \cdot \nabla \mathbf{u} = -\nabla p + \nu \Delta \mathbf{u} + \mathbf{f}, \quad (1)$$

where \mathbf{u} is the velocity, p is the pressure, ν is the molecular viscosity and \mathbf{f} is the forcing. In a typical situation, the forcing is provided by some boundary conditions (experiments) or externally fixed, e.g. by keeping a fixed low-wavenumber Fourier mode at a constant amplitude (numerical simulation). This situation typically gives rise to quasi-Gaussian large-scale velocity fields, while smaller-scale velocities display increasingly non-Gaussian statistics. Presence of the forcing guarantees existence of a stationary steady state in which the total energy is constant. In absence of forcing, the turbulence energy decays steadily, due to losses through viscous effects. However, starting from a quasi-Gaussian large-scale field, one can still observe development of increasingly non-Gaussian small scales in the early stage of the decay. We will study the effect of the non-local interactions on the statistics of such non-Gaussian small scales. For this, we introduce a filter function $G(\mathbf{x})$ in order to separate the large and small scales of the flow. In our numerical

procedure, the filter G will be taken as a cut-off. We have checked that the results are insensitive to the choice of the filter, provided the latter decays fast enough at infinity. Using the filter, we decompose the velocity field into large scale and small scale components:

$$\begin{aligned}\mathbf{u}(\mathbf{x}, t) &= \mathbf{U}(\mathbf{x}, t) + \mathbf{u}'(\mathbf{x}, t), \\ \mathbf{U}(\mathbf{x}, t) &\equiv \bar{\mathbf{u}} = \int G(\mathbf{x} - \mathbf{x}')\mathbf{u}(\mathbf{x}', t)d\mathbf{x}'.\end{aligned}\quad (2)$$

Equations for the large scales of motion are obtained by application of the spatial filter (2) to the individual terms of the basic equations (1). They are:

$$\begin{aligned}\partial_j U_j &= 0, \\ \partial_t U_i + \partial_j \overline{U_i U_j} + \partial_j \overline{U_i u_j} + \overline{U_j u_i} + \partial_j \overline{u_i u_j} &= \\ &= -\partial_i P + \nu \Delta U_i + F_i,\end{aligned}\quad (3)$$

In these equations, we have dropped primes on sub-filter components for simplicity; this means that from now on, any large-scale quantities are denoted by a capital letter, while the small-scale quantities are denoted by a lower case letter. Equation for the small-scale component is obtained by subtracting the large-scale equation from the basic equations (1); this gives

$$\begin{aligned}\partial_j u_j &= 0, \\ \partial_t u_i + \partial_j \left((U_i + u_i)(U_j + u_j) - \overline{(U_i + u_i)(U_j + u_j)} \right) &= \\ &= -\partial_i p + \nu \Delta u_i + f_i,\end{aligned}\quad (4)$$

Several terms contribute to the interaction of scales: *non-local* terms, involving the product of a large scale and a small scale component, and a *local* term, involving two small-scale components. One way to study the dynamical effect of these contributions at small scale, is to integrate numerically a set of two coupled equations, in which the local small scale interactions have been switched off at the small scales ¹. This corresponds to the following set of equations,

$$\partial_t U_i + \partial_j \overline{U_i U_j} = -\partial_j \overline{U_i u_j} - \partial_j \overline{U_j u_i} - \partial_j \overline{u_i u_j}$$

¹We do not switch off the local interactions at the large scales: this would hinder the cascade mechanism and prevent small scale generation from an initial large scale field.

$$-\partial_i P + \nu \Delta U_i + f_i \quad (5)$$

$$\partial_t u_i + \partial_j (U_i u_j) + \partial_j (u_i U_j) = -\partial_i p + \nu \Delta u_i + \sigma_i, \quad (6)$$

$$\partial_j U_j = \partial_j u_j = 0,$$

where

$$\sigma_i = \partial_j \left(\overline{U_i U_j} - U_i U_j + \overline{u_j U_i} + \overline{U_j u_i} \right). \quad (7)$$

The later describes a forcing of the small scales by the large scales via the energy cascade mechanism. This term is always finite even when the external forcing \mathbf{f} (which is always at large scales) is absent. The small scale equation is linear and it resembles the equations of the Rapid Distortion Theory [47]. We shall therefore refer to this new model as the RDT model. The corresponding solution was then compared with a reference simulation performed at the same resolution, with the same initial condition. Note that this comparison is rather expensive numerically: splitting the equations of motions between resolved and sub-filter component leads to additional Fourier transforms, and increases the computational time by a factor 3. This sets a practical limitation to the tests we could perform on our workstation. Also, an additional limitation came from the need of scale separation between the "large" and the "small" scales. This scale separation is mandatory in order to define "non-local" interactions. Their influence on anomalous scaling can be checked only if the typical small scale lies within the inertial range. For this reason, we were led to consider a situation of decaying (unforced) 3D turbulence, with a flat energy spectrum at large scale, and an "inertial range" mostly concentrated at small to medium scales ($10 < k < 40$ for a 256^3 simulation). Indeed, at the resolution we could achieve, forced turbulence developed an inertial range of scale around $k = 8$, too small for the scale separation to be effective (see [29] for a study and discussion of this case and its relevance to LES simulations). Decaying turbulence does not, by definition, achieve a statistically stationary state, with mathematically well defined stationary probability distribution functions (PDF). Therefore, all the PDF were computed at a fixed time which we have chosen to be at the end of each simulation (at $t=0.48$).

1.2 The numerical procedure

1.2.1 The numerical code

Both the Navier Stokes equation (1) and the set of RDT equations (6) were integrated with a pseudo-spectral code (see [49] for more details on the code). In the RDT case, a sharp cut-off in Fourier space was used to split the velocity field into large and small-scale components in Fourier space and all non-linear terms were computed separately in the physical space. The aliasing was removed by keeping only the 2/3 largest modes corresponding to the 85 first modes in our case. The calculations presented here were done with 256^3 Fourier modes and a viscosity of $1.5 \cdot 10^{-3}$ corresponding to a Reynolds number $57 < R_\lambda < 80$ (where R_λ is the Reynolds number based on the Taylor micro-scale λ).

1.2.2 The simulations

The test was performed in a situation of decaying turbulence where the forcing term f_i is set to zero. The initial condition was computed by a direct simulation using a Gaussian velocity distribution as a starting field. We have chosen the velocity field after several turnover times to be the initial condition for our simulations: the direct numerical simulation (DNS), the RDT simulation (eq. 6) and the “local” experiment (see the end of this section). In order to allow enough energy at the large scales, the sharp cut-off filter was taken at the wavenumber $k = 24$ corresponding to approximately 5 Kolmogorov scales. Because of the very low speed of the RDT simulation (three times more expensive than the DNS) the two simulations were performed between $t=0$ and $t=0.48$ corresponding to approximately 2.5 turnover times.

1.3 Comparison of the RDT and DNS experiments

1.3.1 Spectra

The comparison of spectra is shown in Fig 1. In the DNS case, one observes a classical evolution, in which the large scale energy decays while the inertial $k^{-5/3}$ range tends to move towards smaller scales. It can be seen that the inertial range (characterized by the $-5/3$ slope) only marginally exists. In the RDT case, one observes a similar evolution at large scale, while a tendency

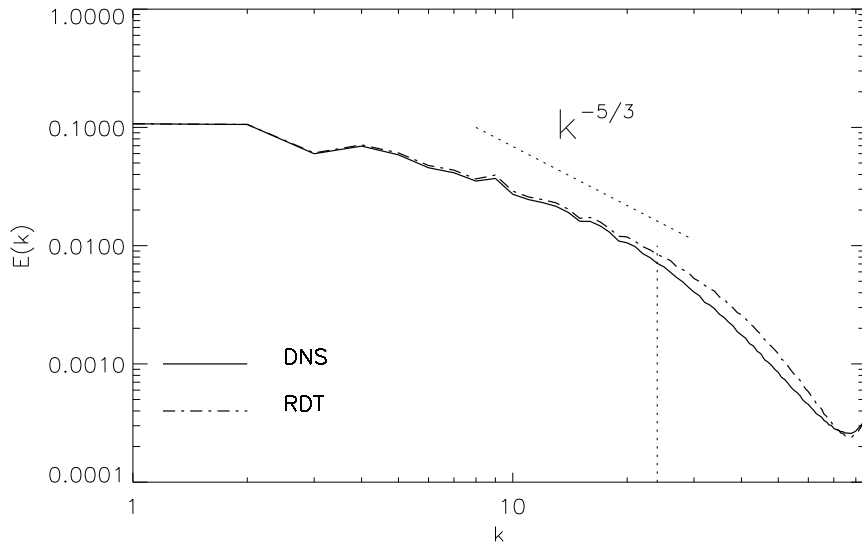


Figure 1: Comparison of energy spectra at $t=0.48$ obtained via the DNS and the RDT simulation.

towards a flatter spectrum is observed near and beyond the separating scale (beyond which local interactions are ignored). We checked that this behavior is not sensitive to the resolution.

The range of computed scales is insufficient to find a reliable value of the spectral slope in the RDT case. However, this slope can be predicted by a simple dimensional argument. This argument was presented for the 2D case in [39], but it is essentially the same for 3D. Indeed, in the RDT case the small-scale equations are linear and, therefore, the energy spectrum $E(k)$ must be linearly proportional to the energy dissipation rate, ϵ . In this case, the only extra dimensional parameter (in comparison with the local/Kolmogorov case) is the large-scale rate of strain α . There is the only dimensional combination of ϵ , α and wavenumber k that has the dimension of $E(k)$; this gives

$$E_k = \frac{C\epsilon}{\alpha} k^{-1}, \quad (8)$$

where C is a non-dimensional constant. In our case, our resolution is too low to be able to check whether the RDT spectrum follows a k^{-1} law, but

we clearly see the tendency to a flatter than $-5/3$ slope. The RDT case is reminiscent of the boundary layer, in which a k^{-1} spectra have been observed [41]. This is not surprising because presence of the mean shear increases the non-locality of the scale interactions corresponding to RDT. In fact, an exact RDT analysis of the shear flow does predict formation of the k^{-1} spectrum [36].

1.3.2 Structures

3D turbulence is characterized by intense thin vortex filaments (“tornadoes”) [44, 49, 50, 43]. Their radii are of order of the dissipative (Kolmogorov) scale which in this case is determined by the balance of the large-scale straining and viscous spreading. In this respect, these vortices are similar to the classical Burgers vortex solution. Fig. 2 shows a comparison of the “tornadoes” observed in the DNS and in the RDT which visualized by plotting surfaces of strong vorticity ($|\omega| > 3.5 \omega_{rms}$). In both cases, thin filamentary structures are observed, but they appear to be much more numerous in the RDT case. Obviously, local interactions tend to dissipate the “tornadoes” which can be interpreted as a mutual distortion and entanglement of “tornadoes” preventing their further stretching by the large scales. On the macroscopic level, this can be regarded as an additional, “turbulent”, viscosity produced by the local interactions. This is compatible with the flattening of the energy spectrum in the RDT case, which we interpreted above in terms of the turbulent viscosity effect.

It is interesting that the Burgers vortex is essentially a linear solution because of the cylindrical shape of this vortex which prevents appearance of the quadratic (in vorticity) terms. Such a linearity is a typical feature of all RDT solutions. On the other hand, there is another candidate which has often been considered to be responsible for intermittency: this is a vortex reconnection process which is believed to lead to a finite time singularity formation (at least for inviscid fluids). Note that the vortex reconnection is an essentially nonlinear process in which the local scale interactions are playing an important role and cannot be ignored. Indeed, there is no finite time blow-up solutions in linear RDT. Likewise, the vorticity grows only exponentially in the Burgers vortex and it does not blow up in a finite time. From this perspective, our numerical results show that the local (vortex-vortex) interactions mostly lead to destruction of the intense vortices and

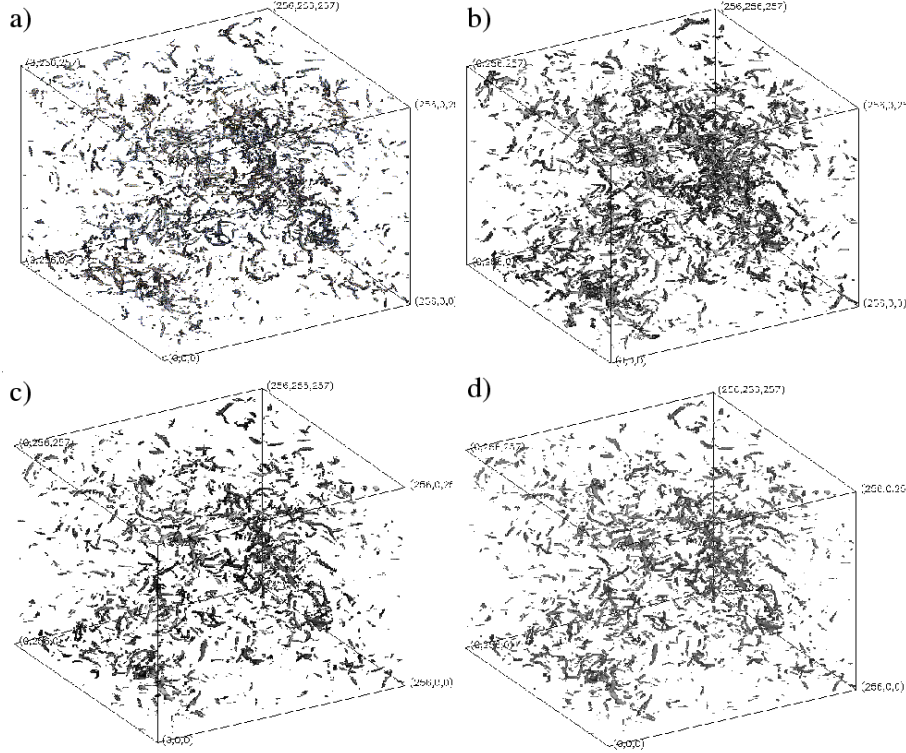


Figure 2: Comparison of vortex structures (isoplot of vorticity $|\omega| = 3.5 \omega_{RMS} = \omega_c$ at $t=0.48$) for a) DNS, b) RDT, c) RDT + constant turbulent viscosity, d) RDT + the RNG-type turbulent viscosity. The number of “tornadoes” estimated by $N = \int_{\omega_c}^{\infty} pdf(|\omega|) d\omega$ are respectively 8245 (a), 21669 (b), 10226 (c) and 10779 (d).

prevention of their further Burgers-like (exponential) growth which has a negative effect on the intermittency. This process seems to overpower the positive effect of the local interactions on the intermittency which is related to the reconnection blow-ups. At the moment, it is not possible to say if the same is true for much higher Reynolds number flows.

1.3.3 Turbulent viscosity

Comparison of the DNS and RDT results for the time evolution of the total energy is shown in (Fig. 3). One clearly observes a slower decline of the total

energy in the RDT case, as if there was a lower viscosity. This results is not

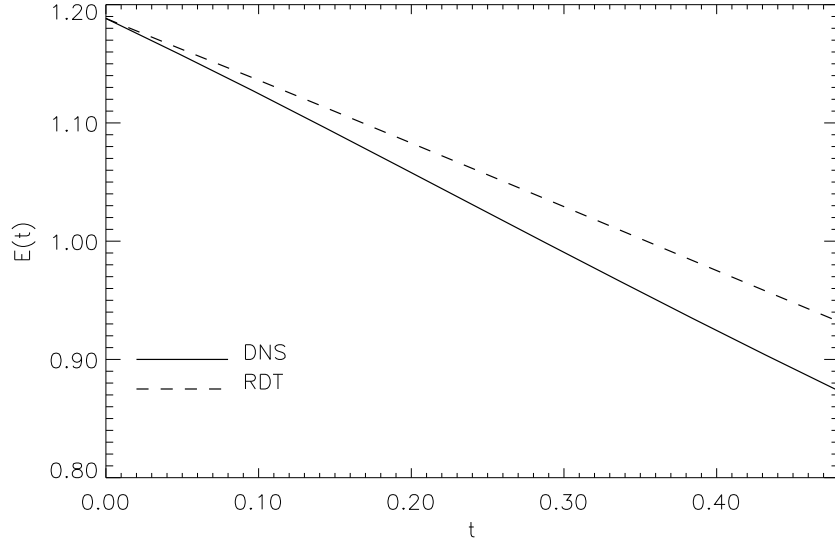


Figure 3: Comparison of the time evolution of total energy.

surprising: it is well known that the influence of energy motions onto well separated large scales (see [27, 18, 51] for systematic expansions) is through an effective eddy viscosity, supplied by the $\langle uu \rangle$ term. Our result suggests that, to a first approximation, the difference between the RDT and the DNS could be removed by including an additional "turbulent" viscosity in the RDT simulation. For the sake of simplicity, we decided to choose an isotropic tensor, chosen as to conserve the total energy. We tried two simple viscosity prescription: one in which ν_t is constant, and one (Fig. 4) in which the viscosity prescription follows the shape dictated by Renormalization Group Theory (see e.g. [9]):

$$\nu_t(k) = \left(\nu^2 + A \int_k^{+\infty} q^{-2} E(q) dq \right)^{1/2} - \nu \quad (9)$$

The constants were adjusted as to obtain a correct energy decay (Fig. 5). They are $\nu_t = 0.0002$ for the constant ν_t prescription, and $A = 0.02$ for the other one. We elaborate more on the choice of this turbulent viscosity

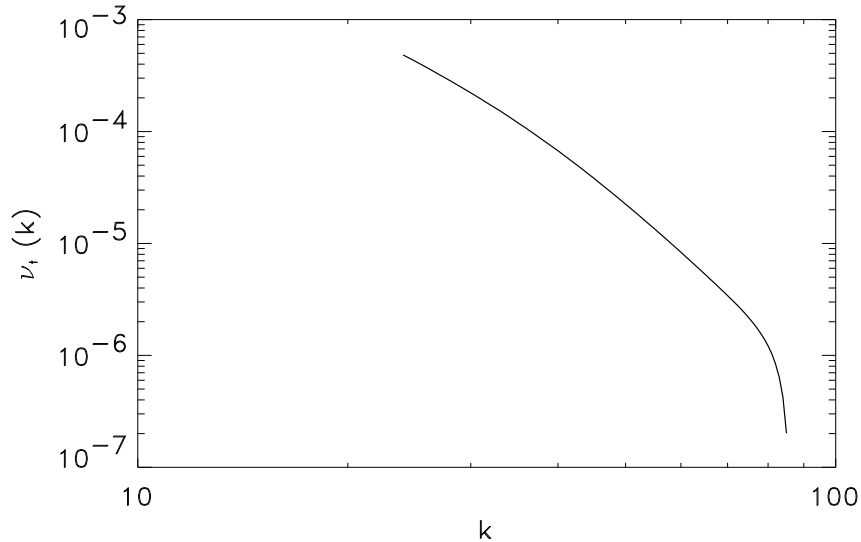


Figure 4: Spectrum of the turbulent viscosity computed by (9) at $t=0.48$

in Section 2.3. Yet another method we tried was to replace the neglected nonlinear term (interaction of small scales among themselves) with its mean value. Dividing this mean nonlinear term by k^2 for each k one can compute the turbulent viscosity $\nu_t(k)$. The result is interesting: ν_t turns out to be nearly independent of k ; this provides an extra justification for the simple model in which $\nu_t = \text{const}$.

The energy spectra and energy decay obtained with this new RDT simulation are shown on Figs. 6 and 5. One sees that one now captures exactly the energy decay of the DNS. The energy spectra become closer to the DNS result at low and intermediate k , whereas at the high k they depart from DNS indicating an over-dissipation of the smallest scales. The later is an artifact of our crude choice for the turbulent viscosity ignoring its anisotropy and possibility for it to take negative values. The turbulent viscosity also influences the anomalous corrections, as we will now show it.

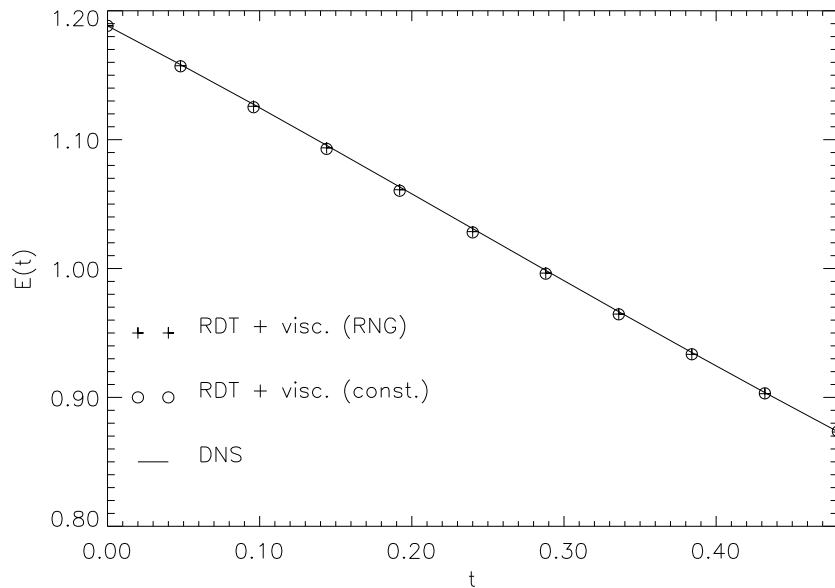


Figure 5: Time evolution of total energy obtained via the DNS and the RDT simulation with the two different turbulent viscosities.

1.3.4 PDF's and exponents

We conducted a statistical study of our velocity fields corresponding to the end of the simulations ($t = 0.48$). As usual for study of the anomalous properties of turbulence, we consider the velocity increments over a distance \mathbf{l} ,

$$\delta\mathbf{u}_{\mathbf{l}} = \mathbf{u}(\mathbf{x} + \mathbf{l}) - \mathbf{u}(\mathbf{x}). \quad (10)$$

As usual, we will deal with the longitudinal and transverse to \mathbf{l} velocity increments, $\delta u_{l\parallel} = (\delta\mathbf{u}_{\mathbf{l}} \cdot \mathbf{l})/l$ and $\delta u_{l\perp} = (\delta\mathbf{u}_{\mathbf{l}} \times \mathbf{l})/l$ respectively, where $l = |\mathbf{l}|$. Figs. 7, 8 and 9 show the probability distribution functions (PDF) of the longitudinal increments and Figs. 10, 11 and 12 the PDF of transverse increments, for 3 values of l , obtained by the DNS, and our different RDT simulation (with and without turbulent viscosity).

At large scale, one observes a quasi-Gaussian behavior, with the development of wider tails as one goes towards smaller, inertial scales. This widening of the PDF's is a classical signature of the anomalous scaling observed in tur-

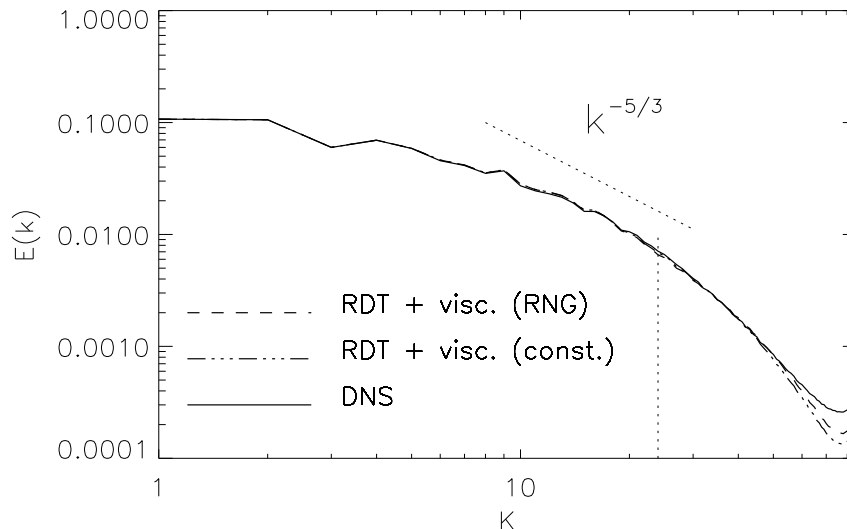


Figure 6: Comparison of energy spectra obtained via the DNS and the RDT simulation with two different forms of the turbulent viscosity

bulence. It can be measured by studying the scaling properties of the velocity structure functions,

$$S_p(\ell) = \langle \delta u_\ell^p \rangle . \quad (11)$$

In the inertial range, the structure function vary like ℓ^{ζ_p} . For low Reynolds number turbulent flows, the scaling behavior in the inertial range is very weak or undetectable because the inertial range is very short. To exemplify this point, we show in Fig. 13 and 14 the structure functions as a function of the scale separation for the longitudinal and the transverse velocity increments (the structure functions from the RDT simulation were shifted by a factor 10 for the clarity of the figures). Given the very weak scaling of our structure functions, we may use the extended self-similarity (ESS) property [5], which states that $S_p(\ell) \sim S_3^{\zeta_p/\zeta_3}$ even outside the inertial range of scales. We use this property because it allows to find the scaling exponents in a more unambiguous way [5]. The measured exponents in our DNS are shown in Fig 15 and in Table 1. In both the longitudinal and transverse case, they are in agreement with the previously reported exponents [3] and they dis-

Table 1: scaling exponent of the velocity structure functions measured using the ESS property, in various simulations, at $t=0.48$.

	longitudinal					
Order	K41	DNS	RDT	RDT + Visc. 1	RDT + Visc. 2	local
1	0.333	0.353	0.361	0.353	0.354	0.344
2	0.667	0.687	0.695	0.687	0.687	0.678
3	1.	1.	1.	1.	1.	1.
4	1.333	1.295	1.273	1.294	1.293	1.310
5	1.667	1.573	1.509	1.570	1.568	1.607
6	2.	1.836	1.696	1.830	1.824	1.892
7	2.333	2.085	1.828	2.073	2.064	2.164
8	2.667	2.321	1.919	2.301	2.287	2.423
	transverse					
Order	K41	DNS	RDT	RDT + Visc. 1	RDT + Visc. 2	local
1	0.333	0.375	0.388	0.376	0.376	0.352
2	0.667	0.707	0.721	0.708	0.709	0.685
3	1.	1.	1.	1.	1.	1.
4	1.333	1.258	1.223	1.255	1.253	1.297
5	1.667	1.484	1.390	1.477	1.468	1.578
6	2.	1.680	1.499	1.664	1.645	1.843
7	2.333	1.849	1.560	1.822	1.782	2.094
8	2.667	1.991	1.591	1.952	1.882	2.333

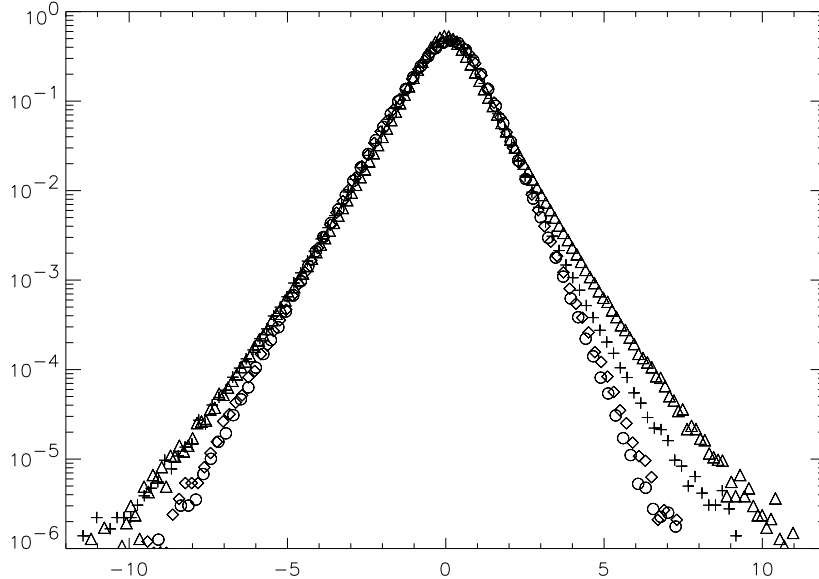


Figure 7: Comparison of the PDF of the longitudinal velocity increments defined by Eq. (10) for $\ell = 2\pi/256$ ($5 \cdot 10^7$ statistics at $t = 0.48$ for the velocity field from the four simulations: DNS (circle), RDT (crosses), RDT + constant viscosity (diamonds) and RDT + viscosity computed from RNG (triangles)

play a clear deviation from the "non-intermittent" value $\zeta_p = p/3$. However the difference between transverse and longitudinal exponents appear to be somewhat larger than the one observed by Dhruva et al [12] and Camussi et al [8]. Corresponding quantities for the RDT simulation are shown in Fig 15 and Table 1. One sees that the RDT statistics display larger and more intermittent PDF tails for small scales, which makes the scaling exponents to take smaller values corresponding to larger anomalous corrections. Again, this situation is reminiscent of the case of the boundary layer. In fact, the measured values in our simulation are remarkably similar to those reported in the atmospheric boundary layer [12] or in a turbulent boundary layer [45]. They are in between the values two different values measured by Toschi ([46]) in and above the logarithmic layer in numerical DNS of a channel flow. A summary of these results is given in Table 2 When a tur-

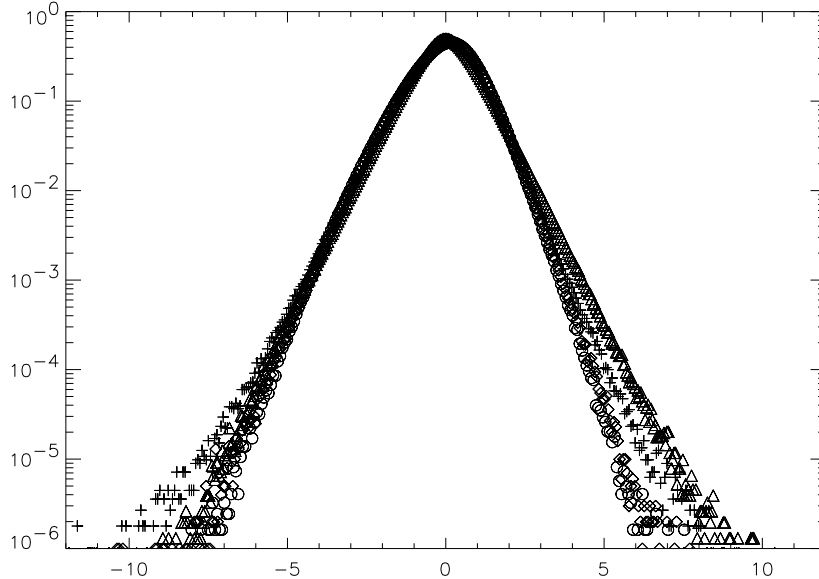


Figure 8: Same caption as in Fig. 7 for $\ell = 2\pi/64$

bulent viscosity is added to the RDT simulation, the intermittent wings are less pronounced in the PDF's and the anomalous correction decrease (Table 1), becoming similar to those observed in the DNS. This agrees with the picture in which the anomalous corrections are determined by the non-local interactions, while the local interactions act to restore the classical Gaussian (Kolmogorov-like) behavior. Obviously, the shape of the turbulent viscosity also influences the intermittency correction: for the transverse case, where there is no asymmetry of the PDF's, both the constant turbulent viscosity and the RNG turbulent viscosity provide intermittency corrections which are of the same level as the DNS. This is quite remarkable, since they include only one adjustable parameter, tuned as to conserve the total energy. For the longitudinal case, where an asymmetry is present, the two prescription give noticeably different result: as one goes towards lower scales, and as the asymmetry becomes larger between the positive and the negative increments, the PDF's computed with RDT and constant turbulent viscosity display tails which are very close to that of DNS, while the PDF's of the RDT with turbulent RNG viscosity have a tendency towards a symmetrical shape, thereby

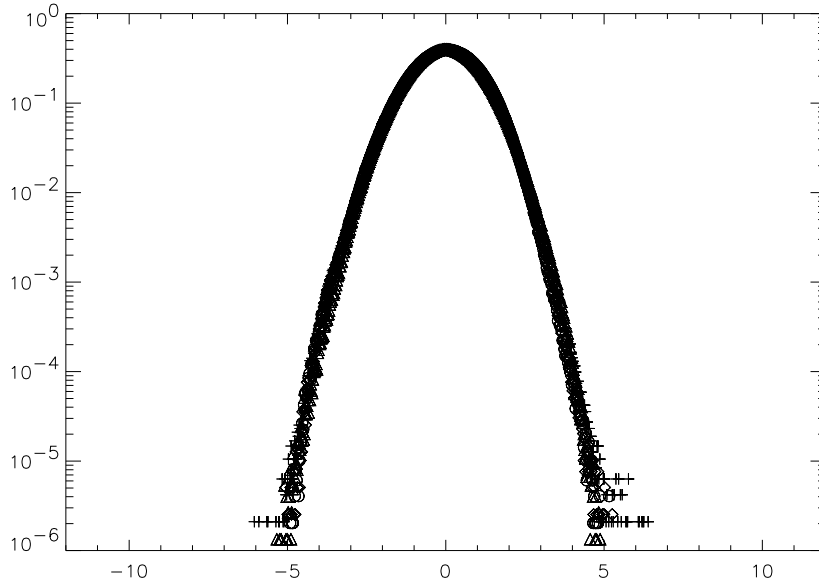


Figure 9: Same caption as in Fig. 7 for $\ell = 2\pi/4$

failing to reproduce the DNS behavior. This difference of behavior between the RNG and constant turbulent viscosity will be further investigated in Section 2.

1.4 Comparison of the “local” experiment with DNS

Given the comparison of the DNS and the RDT (“non-local”) simulation, one could argue that the increase of the intermittency in RDT is mostly due to the increased mean intensity of the small scales (which is seen on the energy spectrum plot). A similar increase of the small-scale intensity could be produced by other means which have nothing to do with non-locality, e.g. by reducing viscosity in DNS. Will there be stronger intermittency in all of such cases too? In order to prove that it is not the case, we perform a simulation where, as the opposite of the RDT one, the non-local interactions at small scales were removed from the NS equation and only the local interactions were retained. In order to keep the local interactions which involve scales close to the cutoff scales, the velocity and the vorticity fields were split into

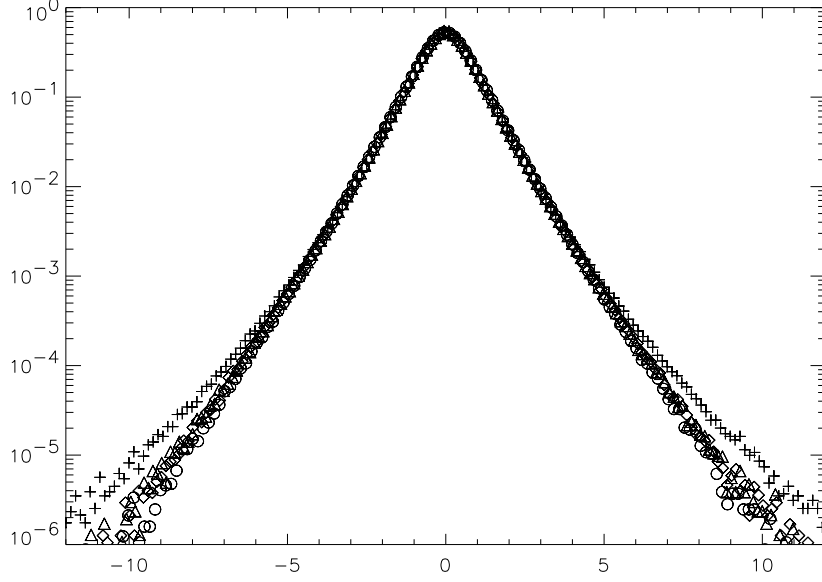


Figure 10: Comparison of the PDF of the transverse velocity increments defined by Eq. (10) for $\ell = 2\pi/256$ (10^8 statistics at $t = 0.48$ for the velocity field from the four simulations: DNS (circles), RDT (crosses), RDT + constant viscosity (diamonds) and RDT + viscosity computed from RNG (triangles)

three parts: the large scales, the medium scales near the cutoff, and the small scales. This decomposition is defined in Fourier space as follows,

$$\mathbf{u}(\mathbf{k}) = \mathbf{u}_{ls}(\mathbf{k}) + \mathbf{u}_{ms}(\mathbf{k}) + \mathbf{u}_{ss}(\mathbf{k}), \quad (12)$$

$$\omega(\mathbf{k}) = \omega_{ls}(\mathbf{k}) + \omega_{ms}(\mathbf{k}) + \omega_{ss}(\mathbf{k}) \quad (13)$$

where

$$\begin{aligned} \mathbf{u}_{ls}(\mathbf{k}) &= \mathbf{u}(\mathbf{k}) && \text{for } k < k_c/C \\ &= 0 && \text{for } k > k_c/C \\ \mathbf{u}_{ms}(\mathbf{k}) &= \mathbf{u}(\mathbf{k}) && \text{for } k_c/C < k < C k_c \\ &= 0 && \text{for } k_c/C < k \text{ and } k > C k_c \\ \mathbf{u}_{ss}(\mathbf{k}) &= \mathbf{u}(\mathbf{k}) && \text{for } C k_c < k \\ &= 0 && \text{for } k > C k_c \end{aligned} \quad (14)$$

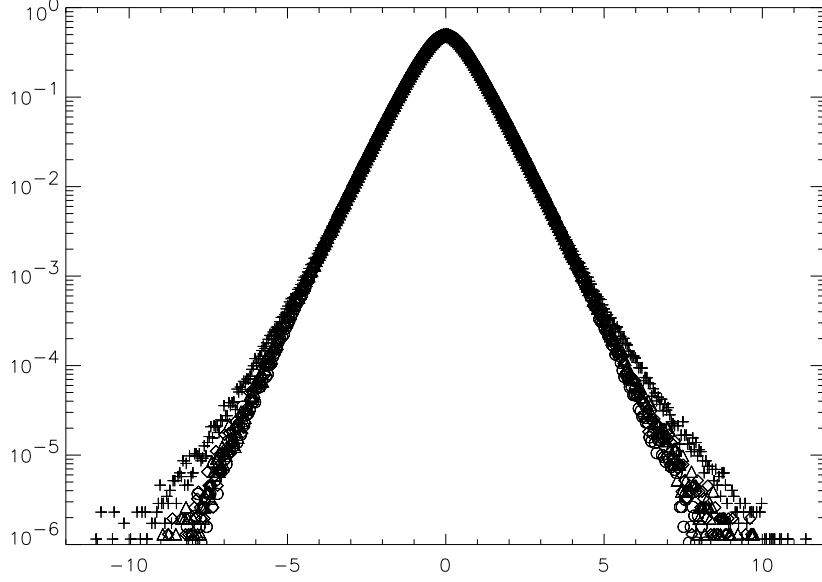


Figure 11: Same caption as in Fig. 10 for $\ell = 2\pi/64$

Using these definition, the equation for the “local” simulation was the following:

$$\begin{aligned} \partial_t \mathbf{u}(\mathbf{k}) + P(\mathbf{u} \cdot \nabla \omega)(\mathbf{k}) \\ - [P(\mathbf{u}_{ls} \cdot \nabla \omega_{ss})(\mathbf{k}) + P(\mathbf{u}_{ss} \cdot \nabla \omega_{ls})(\mathbf{k})]_{\{k > k_c\}} = \nu \Delta \mathbf{u}(\mathbf{k}) \end{aligned} \quad (15)$$

Where P is the projector operator. In our simulation we choose $C = 1.2$ and the same cutoff scale $k_c = 24$. The result of this simulation are compared to the equivalent results from the DNS and the RDT simulation. The energy spectra are compared in Fig. 16. This “local” simulation contain more energy at small scales than the DNS even the RDT. The bump of energy near the cutoff scale k_c is due to the fact that the “local” approximation is introduced only for scales smaller than k_c . Despite the high level of energy at small scales, the solution of this “local” simulation is much less intermittent than the equivalent field from DNS and RDT. A comparison of the scaling exponents is shown Fig. 17 and table 1 for both the longitudinal and transverse velocity increments. These results confirm the idea that intermittency

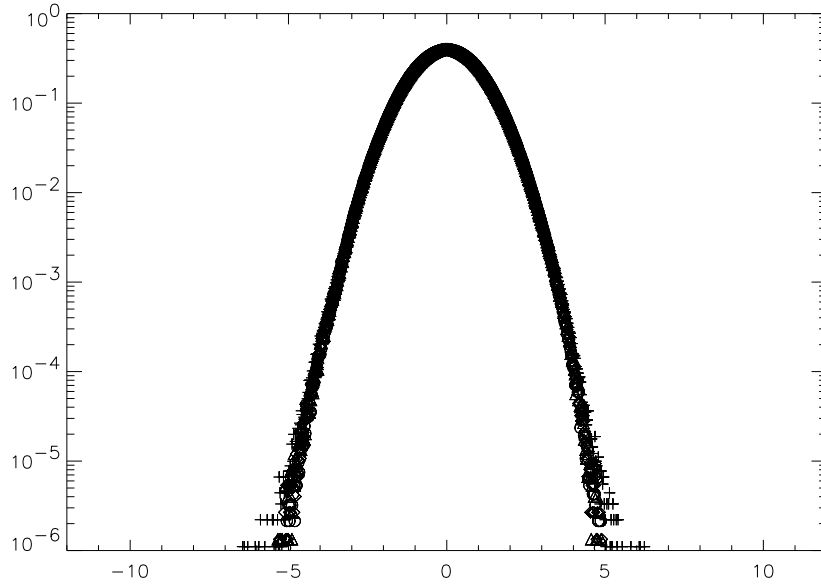


Figure 12: Same caption as in Fig. 10 for $\ell = 2\pi/4$

is caused by the non-local interactions and not just by mere presence of the small scales.

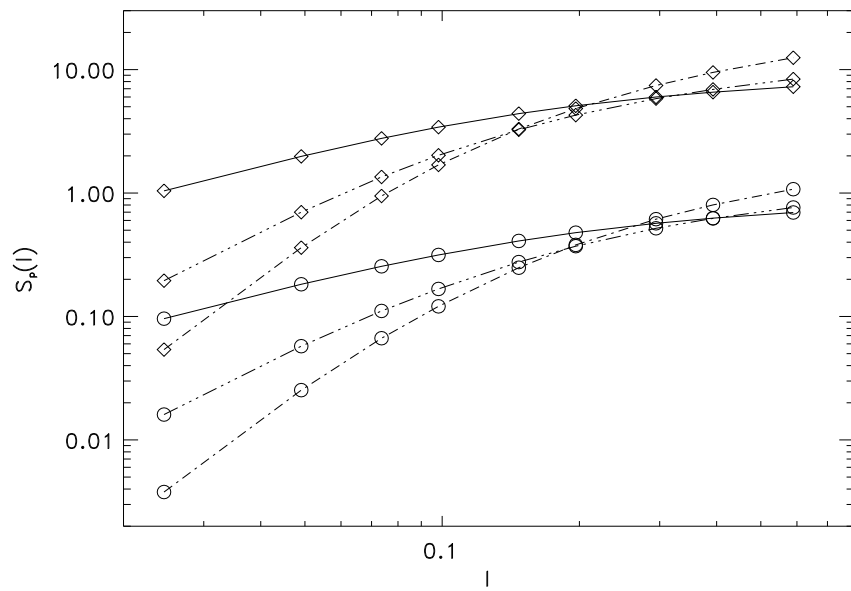


Figure 13: Structure functions computed with the PDF of the longitudinal velocity increments from DNS (circles) and the RDT (diamonds) for the first (solid line), second (dash-dotted line) and third (dash-dot-dot line) moments (for convenience of presentation, the RDT structure functions have been multiplied by 10)

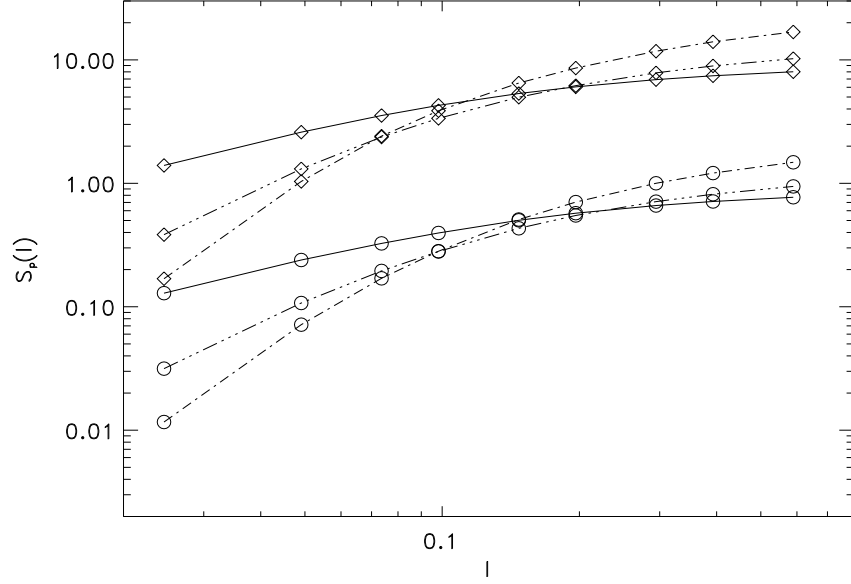


Figure 14: Same plot as in the Fig. 13 for the transverse velocity increments

Table 2: scaling exponents of the velocity structure functions from : atmospheric turbulence at $10000 < R_\lambda < 15000$ (Dhruva) [12], channel flow (Toschi) [46] near the wall ($20 < y^+ < 50$) and far from the wall ($y^+ > 100$) at $Re = 3000$ and boundary layer at $R_\delta = 32000$ (Zubair) [45, 54]

Order	longitudinal				transverse
	Dhruva	Zubair	Toschi $20 < y^+ < 50$	Toschi $y^+ > 100$	Dhruva
1	0.366	-	0.44	0.37	0.359
2	0.700	0.70	0.77	0.70	0.680
3	1.000	1.00	1.00	1.00	0.960
4	1.266	1.20	1.17	1.28	1.200
5	1.493	1.52	1.31	1.54	1.402
6	1.692	1.62	1.44	1.78	1.567
7	-	1.96	1.55	2.00	-

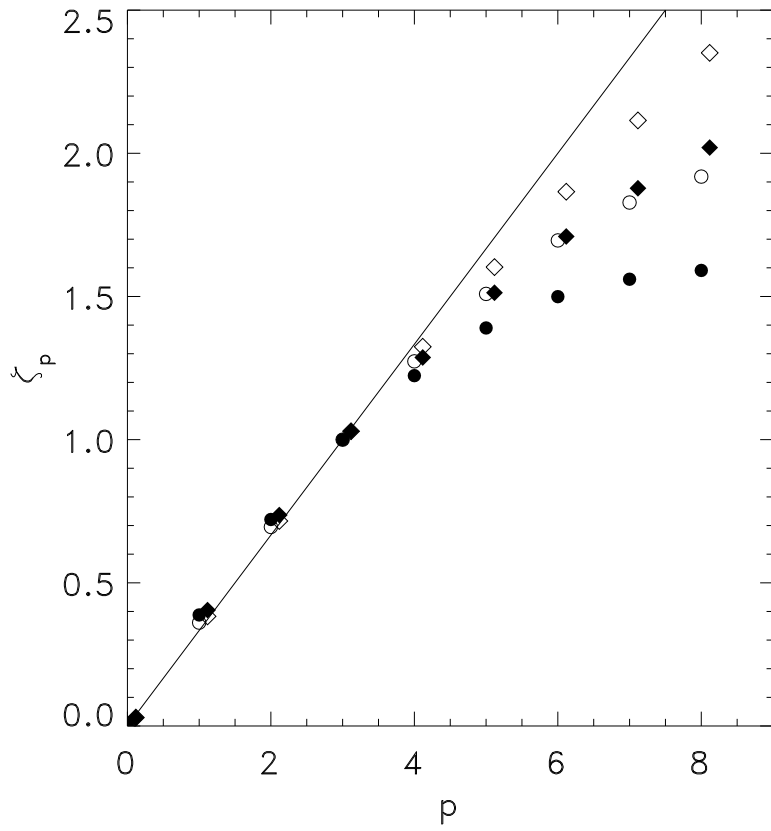


Figure 15: Comparison of the scaling exponents computed from the DNS (diamonds) and the RDT (circles) statistics. The longitudinal exponents are plotted with empty symbols and the transverse exponents with filled symbols.

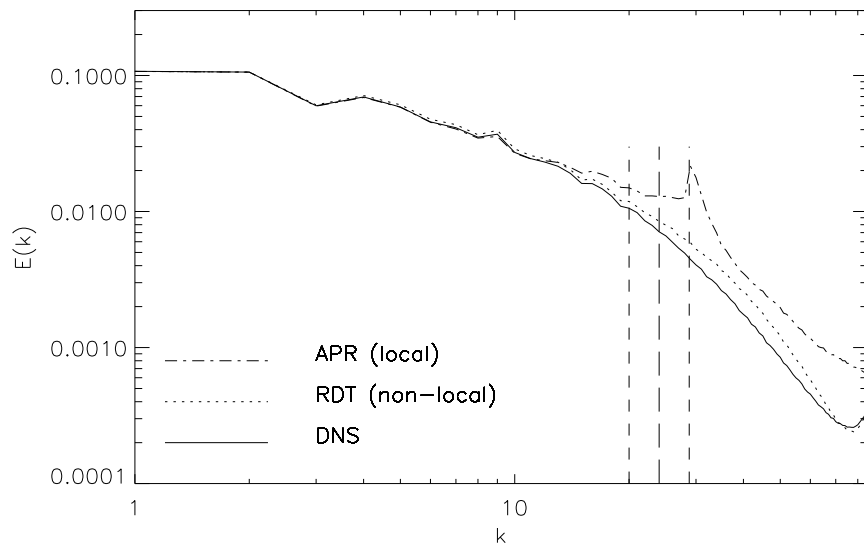


Figure 16: Comparison of energy spectra obtained via the DNS, RDT and the “local” simulation at $t=0.48$

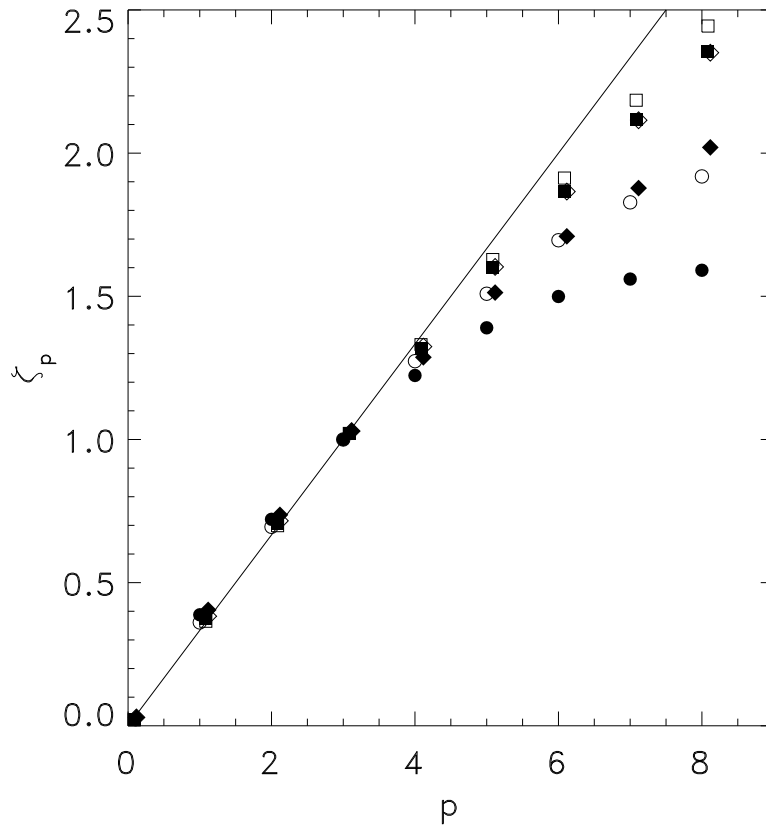


Figure 17: Comparison of the scaling exponents computed from the DNS (diamonds), RDT (circles) and the “local” simulation (squares) statistics. The longitudinal exponents are plotted with empty symbols and the transverse exponents with filled symbols.

2 Qualitative explanation of the intermittency

Our results can be used to get a qualitative understanding of the intermittency via the scale behavior of both the PDF of the velocity increments and its moments. For this, we are going to build a toy model of turbulence, mimicking the small scale non-local dynamics. In spirit, this amounts to an "anti-shell" model of turbulence, because, here, we retain only interactions between distant wave-numbers, by contrast with the ordinary shell model [23, 52, 53] which theoretically only retains local interactions. In this context, it is interesting to note that the ordinary shell model requires a certain degree of non-locality between modes so as to generate intermittency: it can indeed be proven that the intermittency correction disappears when the separation between two consecutive shells tends to zero [14]. Another known pitfall of the shell model is its incapacity to describe the observed skewness (asymmetry) generation along the scale of the PDF of the longitudinal increments. This is annoying, since this skewness is directly related to the non-zero value of the third order moment, and, hence, to the essence of the Kolmogorov cascade picture via the 4/5 law. Finally, the original shell model is very crude, since there is no spatial structure (everything is described by Fourier modes). We now show how elaborate a cleaner toy model of turbulence using localized wave-packets, leading to a description of the small-scale statistics in terms of Langevin processes subject to coupled multiplicative and additive noise.

2.1 The Langevin model of turbulence

Our numerical simulations showed that both the energy spectrum (and decay) and the intermittency quantities are well reproduced by a model in which only the non-local interactions are left in the small-scale equations whereas the local interactions of small scales among themselves are replaced by a turbulent viscosity term. Such a model is described by equations (6) with ν replaced by the turbulent viscosity coefficient ν_t in the small-scale equations,

$$\begin{aligned}\partial_t u_i + \partial_j (U_j u_i) + \partial_j (u_i U_j) &= -\partial_i p + \nu_t \Delta u_i + \sigma_i, \\ \partial_j u_j &= 0,\end{aligned}\tag{16}$$

and σ_i is given by (7). We are interested in the contribution of non-local interactions to the statistics of the non-Gaussian small scales. For this, we assume that the large scale L quantities (\mathbf{U} and its derivative, and σ_i) are fixed external processes, with prescribed statistics (to be defined later), and derive an equation for the small scale \mathbf{l} velocity field \mathbf{u}' , by taking into account the scale separation $\ell/L = \epsilon \ll 1$. For this, we decompose the velocity field into localized wave-packets via a Gabor transform (GT) (see [37])

$$\hat{u}(\mathbf{x}, \mathbf{k}, t) = \int g(\epsilon_* |\mathbf{x} - \mathbf{x}'|) e^{i\mathbf{k} \cdot (\mathbf{x} - \mathbf{x}')} \mathbf{u}(\mathbf{x}', t) d\mathbf{x}', \quad (17)$$

where g is a function which decreases rapidly at infinity and $1 \ll \epsilon_* \ll \epsilon$. Note that the GT of \mathbf{u} is a natural quantity for the description of the velocity increments because of the following relation

$$\mathbf{u}(\mathbf{x} + \mathbf{l}) - \mathbf{u}(\mathbf{x} - \mathbf{l}) = \frac{1}{2i} \int e^{-i\mathbf{k} \cdot \mathbf{l}} \text{Im} \hat{\mathbf{u}}(\mathbf{x}, \mathbf{k}) d\mathbf{k}. \quad (18)$$

Thus, velocity increments are related to GT via the Fourier transform, and all information about the l -dependence is contained in the GT dependence on k (the main contribution to the above integral comes from $k \sim 2\pi/l$). On purely dimensional ground, we see that $\hat{u} \sim k^{-d} \delta u$, where d is the dimension. Therefore, in the sequel, we shall identify $k^d \text{Im} \hat{u}$ with the velocity increment.

Applying GT to (6) we have (see [38] for details):

$$D_t \hat{\mathbf{u}} = \hat{\mathbf{u}} \cdot \hat{\xi} + \hat{\sigma}_\perp - \nu_t k^2 \hat{\mathbf{u}}, \quad (19)$$

where ξ and σ_\perp are random processes, given by

$$\begin{aligned} \hat{\xi} &= \nabla \left(2 \frac{\mathbf{k}}{k^2} \mathbf{U} \cdot \mathbf{k} - \mathbf{U} \right), \\ \hat{\sigma}_\perp &= \hat{\sigma} - \frac{\mathbf{k}}{k^2} (\mathbf{k} \cdot \hat{\sigma}), \end{aligned} \quad (20)$$

and

$$D_t = \partial_t + \dot{\mathbf{x}} \cdot \nabla + \dot{\mathbf{k}} \cdot \nabla_{\mathbf{k}}, \quad (21)$$

$$\dot{\mathbf{x}} = \mathbf{U} = \nabla_k H, \quad (22)$$

$$\dot{\mathbf{k}} = -\nabla(\mathbf{k} \cdot \mathbf{U}) = -\nabla H, \quad (22)$$

$$H = \mathbf{U} \cdot \mathbf{k}. \quad (23)$$

Because the large-scale dynamics is local in k -space, it is only weakly affected by the small scales and the quantities ξ and σ in equation (19) can be considered as a given noise. Also, because the equation is linear in \hat{u} , we immediately see that $k^d \hat{u}$ will also satisfy an equation similar to (19) subject to a straightforward modification of the force definitions. Before elaborating more on (19), it is convenient to study in closer details the physical parameters of this equation.

2.2 The noises

In equation (19), the noise ξ and σ_\perp appearing as the projector of two quantities, one related to the velocity derivative tensor, and another related to the Gabor transform of the energy transfer from large to small scales. In the sequel, we present a statistical study of these two noises in the physical space (i.e. after inverse Gabor transforming $\hat{\sigma}_\perp$). We will also consider the Fourier spectra of the corresponding two-point correlations. Let us choose \mathbf{k} to be along one of the coordinate axis (without loss of generality because of the isotropy). Then the components of ξ coincide (up to the sign) with the corresponding components of the velocity derivative tensor, and we will use this fact in the rest of this section. The velocity derivative tensor has been studied in the literature e.g. in [48, 2] in terms of correlations between the directions of the anti-symmetrical part of the tensor (the vorticity) and the symmetrical part (the strain). Over long time, the vorticity appears to be aligned with the direction of largest stretching. Other studies focused on the PDF of the modulus of one component. For example, Marcq and Naert [32] observe that the derivative has a highly non-Gaussian distribution, but with a correlation function which decays rapidly, and can be approximated by a delta function at scales large compared to the dissipative scale. In the present case, we observe different features. Because of the isotropy, we can concentrate only on two quantities, say ξ_{11} and ξ_{12} . Fig. 18 shows the equal-position, time correlation $C_{1i}(t-t_0) = \langle \xi_{1i}(t)\xi_{1i}(t_0) \rangle$ and $\alpha_{ii}(t-t_0) = \langle \sigma_i(t)\sigma_i(t_0) \rangle$ as a function of $t-t_0$. Note that these quantities are normalized to 1 at $t=t_0$ in this figure. Firstly, we see that C_{11} approximately coincide with C_{12} and α_{11} coincides with α_{22} which is a good indicator of isotropy (without normalization there would be $C_{12} = -3C_{11}$). Secondly, we see that the correlations C_{11} and C_{12} decay to zero over a time scale which is of the order of few turnover times τ ($\tau = 0.19$). On the other hand, the correlations of σ decay much faster,

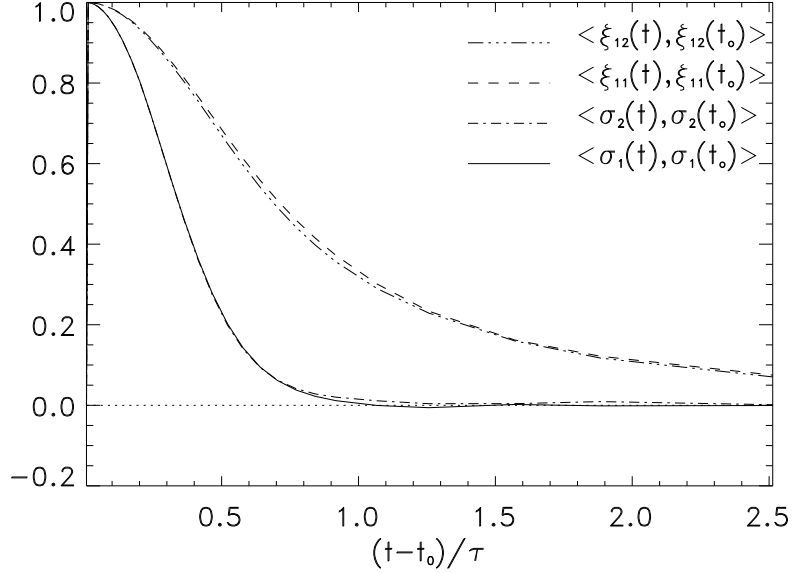


Figure 18: The normalized auto-correlation in time for the two force components σ and ξ (the turnover time τ is equal to 0.19)

over a time of the order of $\tau/2$. Fig. 19 displays the Fourier transforms of the equal-time two-point correlations $D_{1i}(x-x_0) = \langle \xi_{1i}(x, y, z, t) \xi_{1i}(x_0, y, z, t) \rangle$ and $\alpha_{ii}(x-x_0) = \langle \sigma_i(x, t) \sigma_i(x_0, t) \rangle$. One sees that all correlations are very weak beyond $2k_c$. The correlation D_{12} appears to be the largest at large scales, but it decays more rapidly than the other correlations. We have also investigated the cross-correlations between the noises. The equal position cross-correlations are displayed in Fig. 20. The correlation is rather weak, but there is a tendency for σ_i to be correlated with ξ_{1i} over a time scale of the order of τ , while it is anti-correlated with the other component of the tensor, over such a time scale. The equal time correlations are shown in Fig. 21. Notice that the cross correlations are one order of magnitude weaker than the direct correlations. The cross-correlation involving ξ_{12} are essentially zero, while the correlations involving ξ_{11} display a first overall decay up to $k = k_c$, followed by an extra bump up to the end of the inertial range ($k = 40$). In the next Section, we will show that this feature is actually related to the energy cascade.

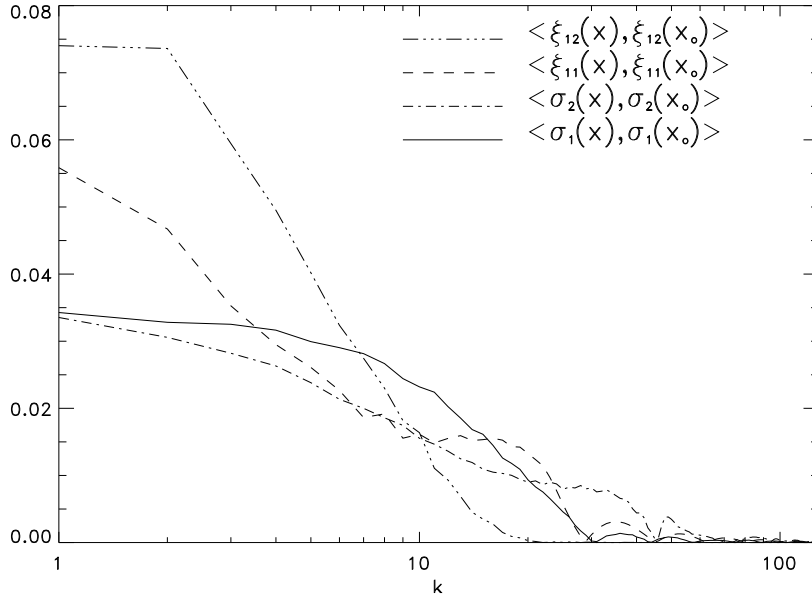


Figure 19: Fourier transform of the space auto-correlation for the two components of the force σ and ξ . Coordinates y and z are fixed.

One may also note that the two noises are spatially very intermittent. In Fig. 22, we show iso-surfaces of the modulus of the noises, corresponding to 3.5 times the RMS value. For comparison, the same plot is made for the vorticity. One observes well defined patches of σ which are strongly correlated with areas of strong vorticity. In the case of ξ , the patches are much more space filling. The longitudinal component ξ_{11} is characterized by smaller-scale structures than the transverse component ξ_{12} .

To obtain an indication about the scale variation of the statistical properties of the noises, we also computed the PDF's of the noise spatial increments $\delta\sigma_{i\ell} = \sigma(x + \ell) - \sigma(x)$ and $\delta\xi_{ij\ell} = \xi_{ij}(x + \ell) - \xi_{ij}(x)$. Note that the first of these quantities is directly related with the Gabor transform of the additive noise, whereas the second one contains some useful information about the time correlations via the Taylor hypothesis (which is valid locally because the large-scale velocity is typically greater than the small-scale one). Fig. 23 shows the results of the longitudinal and transverse increments for the first component of the additive noise σ_1 and the equivalent results for

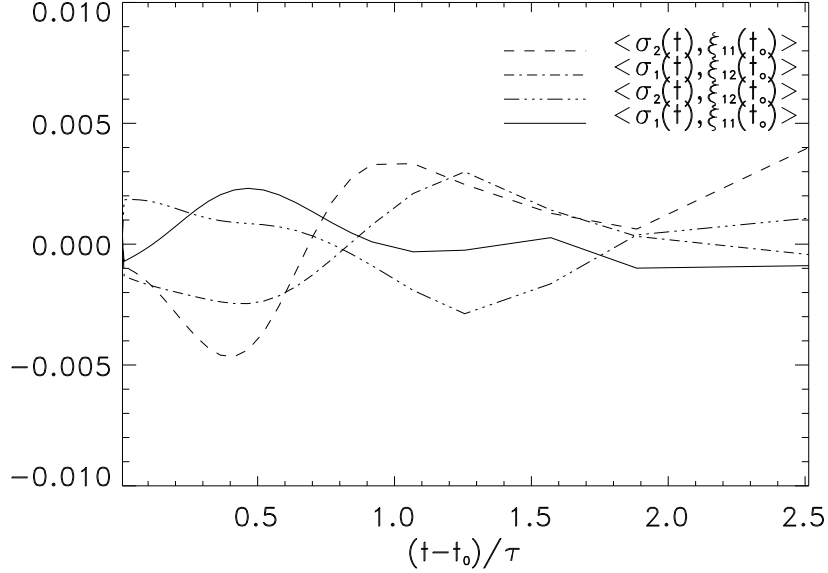


Figure 20: The cross-correlation in time between the forces σ and ξ ($\tau = 0.19$)

the component ξ_{11} of the multiplicative noise are shown on Fig. 24. The PDF are displayed for $\ell = 2\pi/256$ and $2\pi/4$. One observes wide, quasi-algebraic tails for the additive noise, similar to those observed for the PDF's of the velocity derivatives. The PDF of ξ_{11} are much closer to Gaussian statistic.

2.3 The turbulent viscosity

In the previous Section, we have discussed the influence of two prescription for the turbulent viscosity, one based on the RNG, one taken simply as constant. In the sequel, we shall use the simple formula:

$$\nu_t = \left(\nu_0^2 + B^2 \left(\frac{u}{k} \right)^2 \right)^{1/2}, \quad (24)$$

where ν_0 and B are a constant and $u = k^d \text{Im} \hat{u}$ is the velocity increment over a distance $1/k$ (hereafter we drop δ in δu). When $B = 0$, this formula provides the constant turbulent viscosity. When $\nu_0 = 0$, it provides a

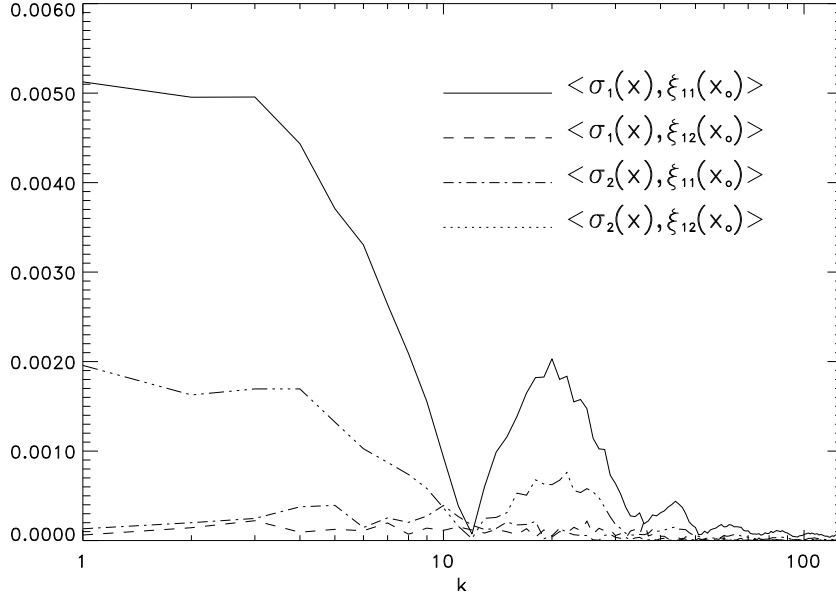


Figure 21: Fourier transform of the space cross correlation between the force σ and the force ξ . Coordinates y and z are fixed.

dimensional analog of the RNG viscosity, and tends to zero as k tends to infinity.

2.4 Statistical properties of the velocity increments

We are now going to derive qualitative results by adopting two complementary points of view: in a first one, we will study the statistical properties of the velocity increments in the frame of reference moving together with the wave packets in (k, x) space. This corresponds to a Lagrangian description in the scale space. In the second approach, we replace time with its expression in terms of k , as it would follow from the ray equation (22). This will give as an equation at a fixed k which corresponds to an Eulerian description. As a further simplification, we shall leave for further study the possible correlation between longitudinal and transverse velocity increments described for example in [1] and consider a one-dimensional version of (19), treating the

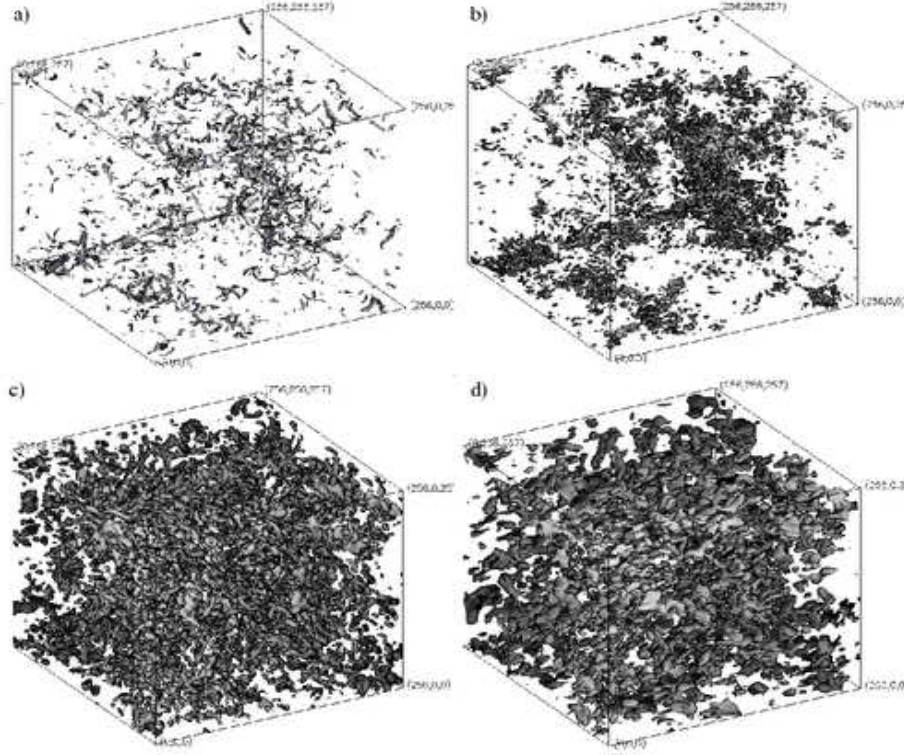


Figure 22: Isovalue (3.5 times the RMS) at $t_0 = 0$ of **a)** the absolute value of vorticity, **b)** the corresponding additive force ($|\sigma|$) **c)** $\xi_{11} = \partial U_x / \partial x$ and **d)** $\xi_{12} = \partial U_x / \partial y$

quantity $u = k \text{Im} \hat{u}$ as a “velocity increment” over the distance $l = 2\pi/k$,

$$D_t u = u\xi + \sigma_\perp - \nu_t k^2 u, \quad (25)$$

$$\dot{k} = -k\xi \quad (26)$$

Here, we assumed that the forcing to be symmetric such that it does not produce any $Re \hat{u}$. This toy model can also be viewed as a passive scalar in a compressible 1D flow. Artificial introduction of compressibility is aimed at modeling the RDT stretching effect which appears only in the higher number of dimensions for incompressible fluids.

Study of the noises in Section 2.2 revealed their rich and complex behavior. As a first simplifying step, we disregard these complexities and use the

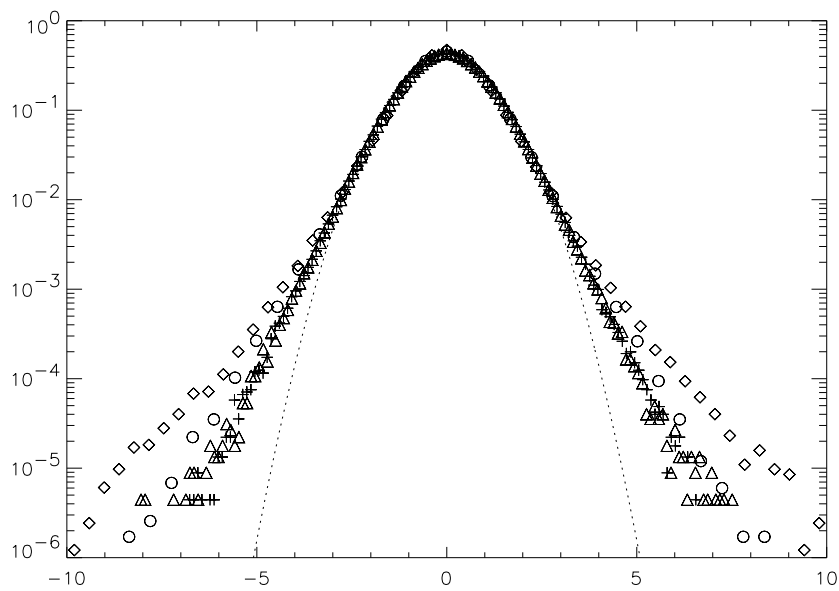


Figure 23: PDF of the increments $\sigma_1(x + \ell_1, y, z) - \sigma_1(x, y, z)$ for $\ell_1 = 2\pi/256$ (circles) and $\ell_1 = 2\pi/4$ (crosses) and $\sigma_1(x, y + \ell_2, z) - \sigma_1(x, y, z)$ for $\ell_2 = 2\pi/256$ (triangles) and $\ell_2 = 2\pi/4$ (diamonds) (the dotted line corresponds to Gaussian statistics).

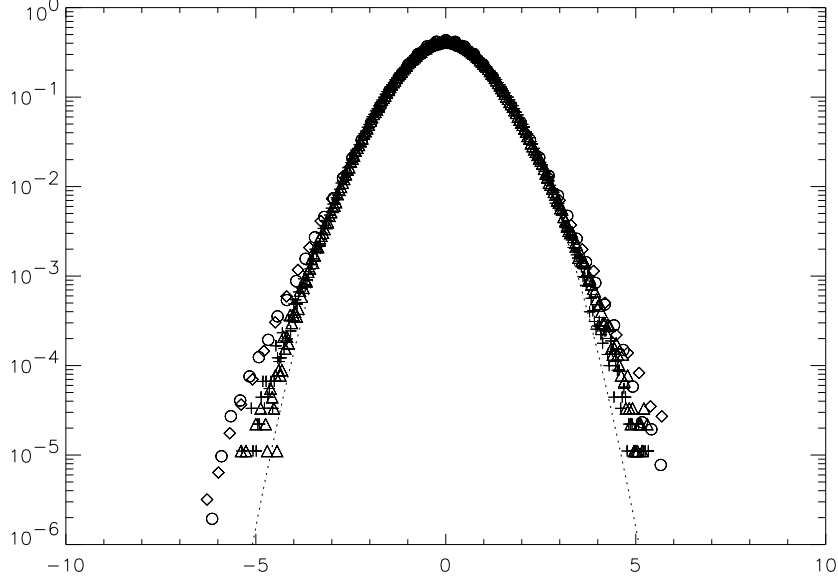


Figure 24: PDF of the increments $\xi_{11}(x+\ell_1, y, z) - \xi_{11}(x, y, z)$ for $\ell_1 = 2\pi/256$ (circles) and $\ell_1 = 2\pi/4$ (crosses) and $\xi_{11}(x, y + \ell_2, z) - \xi_{11}(x, y, z)$ for $\ell_2 = 2\pi/256$ (triangles) and $\ell_2 = 2\pi/4$ (diamonds) (the dotted line corresponds to Gaussian statistics).

Gaussian, delta correlated approximation, as will be done in the next two sub-sections. Given a rather short time correlation of σ , our delta approximation is rather safe. The delta approximation for ξ is more debatable, and the performance of such a model should be further examined in future. Also, the Gaussian hypothesis is obviously only valid at large scale, and for ξ_{11} . Therefore, the generalization of our results for non-Gaussian noises would be very interesting, and is the subject of an ongoing research. In the sequel, we consider the function α , D and λ as free parameters.

2.4.1 The Lagrangian description

In the frame of reference moving with the wave packets in (k, x) space, the l.h.s. of (25) becomes simply the time derivative. On the other hand, k has to be replaced in terms of its initial value k_0 and time everywhere including

the noises σ and ξ . Such a transformation from the laboratory to the moving frame can obviously change the statistics of σ and ξ . In the Lagrangian description we will assume that we deal with noises which are Gaussian in the moving frame with correlations functions

$$\begin{aligned} \langle \sigma_{\perp}(k(t), t) \sigma_{\perp}(k'(t), t') \rangle &= 2\alpha \delta(t - t'), \\ \langle \xi(k(t), t) \xi(k'(t), t') \rangle &= 2D \delta(t - t'), \\ \langle \xi(k(t), t) \sigma_{\perp}(k'(t), t') \rangle &= 2\lambda \delta(t - t'), \end{aligned} \quad (27)$$

where coefficients α , D and λ depend on the scale via k_0 . With these noises, (25) becomes a Langevin equation for the velocity increments, where ξ is a multiplicative noise, σ_{\perp} is an additive noise, and $\nu_t k^2 u$ the (non-linear) friction. The multiplicative noise is produced by interaction of two small scales with one large scale whereas the additive noise is due to a merger of two large scales with into one small scale (therefore, the later acts at the largest among the small scales). For Gaussian, delta correlated noises, this Langevin equation leads to a Fokker-Planck equation for the probability distribution $P_k(u, t)$ of the velocity increment u ,

$$\begin{aligned} \partial_t P_k &= \partial_u \left(\nu_t k^2 u P_k \right) \\ &+ D_k \partial_u (u \partial_u P_k) - \lambda_k \partial_u (u \partial_u P_k) \\ &- \lambda_k \partial_u^2 (u P_k) + \alpha_k \partial_u^2 P_k, \end{aligned} \quad (28)$$

where we have taken into account the fact that, due to homogeneity, ξ and σ have a zero mean. Here, we dropped the the subscript 0 in k_0 and dependence of the all involved quantities on the scale is simply marked by the subscript k (the scale dependence α , D and λ is still unspecified). The stationary solution of (28) is:

$$P_k(u) = C_k \exp \int_0^u \frac{-\nu_t k^2 y - Dy + \lambda}{Dy^2 - 2\lambda y + \alpha} dy, \quad (29)$$

where C_k is a normalization constant. The integral appearing in (29) can be explicitly computed in two regimes: in the first one, for $u \ll k\nu_0$, we have ($\nu_t = \nu_0$), and we simply get

$$P_k(u) = \frac{C}{(Du^2 - 2\lambda u + \alpha)^{1/2 + \nu_0 k^2 / (2D)}}, \quad (30)$$

The range of u for which the PDF follows this algebraic law decreases with increasing scales. It is the largest (and hence it is best observed) at the dissipative scale, where the velocity increments are equivalent to velocity derivative or to vorticity. Several remarks are in order about this expression. First, notice that the distribution is regularized around $u = 0$ by the presence of the parameter α , but then displays algebraic tails. These are well known features of random multiplicative process with additive noise (see e.g [35]). The occurrence of algebraic tails in vorticity PDF's has been noted before by [24, 34] in the context of 2D turbulence. However, processes with algebraic tails are characterized by divergent moments. These divergences can be removed by taking into account finite size effects, like physical upper bounds on the value of the process (see, e.g. [31] for discussion and references) which introduce a cut-off in the probability distribution. This effect is automatically taken into account in our simple model, via the turbulent viscosity, which prevents unbounded growth of velocity fluctuations and introduces an exponential cut-off.

Indeed, in the regime $u \gg k\nu_0$, we see that:

$$\frac{d \ln P}{du} \approx \frac{-u|u|}{Du^2 - 2\lambda u + \alpha}. \quad (31)$$

This mean that at large u the PDF decays like an exponential, or even faster if $D = 0$ (see below). This feature had been noted by Min et al [34], and finds here a detailed explanation.

Another important observation is that the PDF's have an intrinsic skewness, which can be traced back to the non-zero value of λ , i.e. to the correlation between the multiplicative and the additive noise. The physical picture associated with this correlation is related to the correlation between vorticity (present in the large scale strain tensor) and stretching (associated with the term $U\nabla U$, present in σ), which is the motor of the energy cascade [1]. The importance of the additive noise in the skewness generation has been stressed before [16]. We find here its detailed explanation. Note also that the trends towards Gaussian large scale behavior of the velocity increments can be easily accounted for if the multiplicative noise tends to zero at large scale ($D, \lambda \rightarrow 0$). In such case, the process becomes purely additive, and the limiting PDF is Gaussian for u independent turbulent viscosity, or can also fall faster than a Gaussian (like $\exp(-u^3)$, for $\nu_t \propto u$). Such a supra Gaussian behavior has been noted before [1]. In between the dissipative and the largest

scale, the transition operates via PDF's looking like stretched exponential.

This qualitative feature can be tested by comparison with the numerical PDF's. Our model, predicts that $d \ln P/du$ should behave like the ratio:

$$\frac{d \ln P}{du} = \frac{-u\sqrt{(m_1u)^2 + m_2^2} - m_4u + m_3}{m_4u^2 - 2m_3u + m_5}. \quad (32)$$

Without loss of generality, we can factorize out the parameter m_5 . The fit therefore only contains four free parameters, which can be easily related to the physical parameters of the problem. We have computed this derivative for the PDF of longitudinal and transverse velocity increments at various scale, and performed the four parameters fit. Examples are shown on Fig. 25. Observe the good quality of the fit, but we stress that there is a rather large uncertainty in the determination of the parameter of the fits, which sometimes cannot be determined better than up to a factor of two by our fit procedure (a standard least square fit). The scale dependence of the coefficients of the fit, is shown on Fig. 26 and 27. Note that since transverse velocity increments are symmetrical by construction, we have set $m_3 = 0$ in the fit. Note that in the longitudinal case, m_3 is smaller than the other coefficients by two orders of magnitude. This features the smallness of the skewness, and the weakness of the correlation between the multiplicative and the longitudinal noise (see Section 2.1). The parameters have a rough power law behavior (see Fig. 26 and 27). Theoretically, one expects the ratio m_1/m_2 to behave like $1/(\nu_0 k)$, if (24) holds. The power-law fits of Fig. 26 and 27 provides a dependence of $k^{0.53}$ for the longitudinal case, and $k^{-0.54}$ for the transverse case, corresponding to a scale dependence of ν_0 given by $k^{1.53}$ and $k^{0.46}$.

2.4.2 The Eulerian description

We now consider (25), again in the moving with the wave packet frame, but now we change the independent variable from t to $k = k(t)$ which satisfies (26). We get

$$\frac{du}{d \ln k} = -\mathcal{P}u + \frac{\nu_t k^2}{\xi} - \frac{\sigma_\perp}{\xi}, \quad (33)$$

where \mathcal{P} is a number, accounting for the projection operator (a way to mimic higher-dimensional effects in our 1D toy model). Eq. (33) is again a Langevin

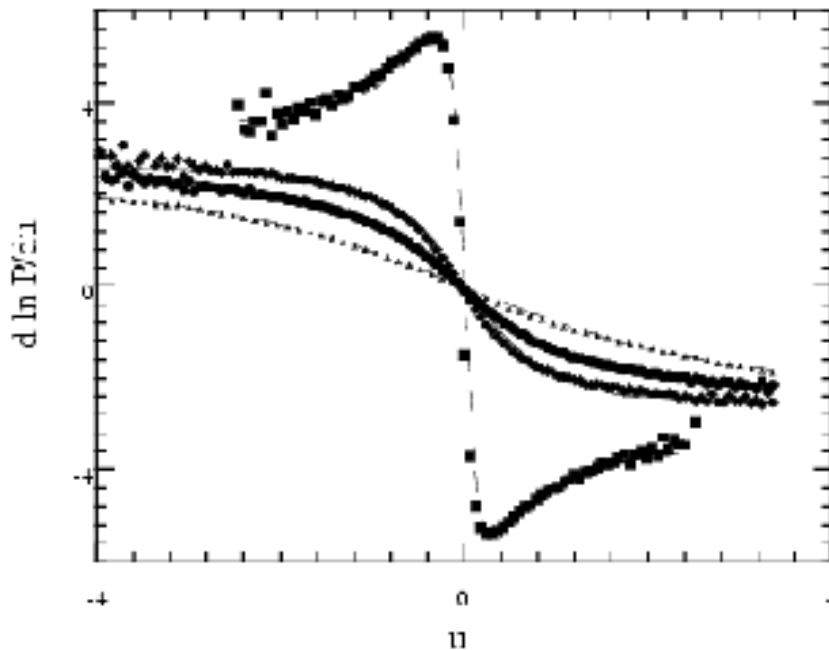


Figure 25: Fit of $d \ln P/du$ for the transverse increments, at $1/k = 2$ (squares), $1/k = 32$ (diamonds), $1/k = 42$ (circles) and $1/k = 52$ (triangles). The fits via formula 32 are given by lines. Note the good quality of the fit. Similar fits for other scale separations, and in the longitudinal case were obtained.

equation for velocity increments in the scale space, with multiplicative and additive noises which is now expressed in an Eulerian form. Similar Langevin processes have been proposed before to explain the scale dependence of velocity increments [20, 33, 32] but without additive noise [19].

The noises in this Langevin equation are different from the noises appearing in the Lagrangian representation and they would have a complicated statistics if we assumed that σ and ξ were Gaussian in the Lagrangian representation. However, we can simply assume here that the noises are Gaussian and delta-correlated in the Eulerian representation (which is different from

the assumption of the previous section) and re-define α , D and λ as

$$\begin{aligned} \langle \sigma_{\perp}(k, t(k)) \xi^{-1}(k, t(k)) \sigma_{\perp}(k', t(k')) \xi^{-1}(k', t(k')) \rangle &= 2\alpha \delta(k - k'), \\ \langle \xi^{-1}(k, t(k)) \xi^{-1}(k', t(k')) \rangle &= 2D \delta(k - k'), \\ \langle \xi^{-1}(k, t(k)) \sigma_{\perp}(k', t(k')) \xi^{-1}(k', t(k')) \rangle &= 2\lambda \delta(k - k'), \end{aligned} \quad (34)$$

This allows one to derive the Fokker-Planck equation corresponding to (33),

$$\begin{aligned} k \partial_k P(u, k) &= \partial_u (\mathcal{P} u P) \\ &+ D \partial_u (\nu_t k^2 u \partial_u [\nu_t k^2 u P]) - \lambda \partial_u (\nu_t k^2 u \partial_u P) \\ &- \lambda \partial_u^2 (\nu_t k^2 u P) + \alpha \partial_u^2 P. \end{aligned} \quad (35)$$

We may use (35) to derive an equation for the moments, by multiplication by u^n and integration over u . With the shape of the turbulent viscosity given by (24), we get:

$$\begin{aligned} k \partial_k \langle u^n \rangle &= -\zeta(n) \langle u^n \rangle \\ &+ n D B^2 k^2 \langle u^{n+2} \rangle - \lambda n (2n - 1) \nu_t k^2 \langle \frac{u^{n-1}}{\nu_t} \rangle \\ &- 2n^2 \lambda B^2 \langle \frac{u^{n+1}}{\nu_t} \rangle + \alpha n (n - 1) \langle u^{n-2} \rangle, \end{aligned} \quad (36)$$

where $\zeta(n) = n\mathcal{P} - n^2 D k^4 \nu^2$ is the zero-mode scaling exponent. For $n = 1$ and taking into account the constraints that $\langle u \rangle = 0$ (homogeneity), one get a sort of generalized Karman-Horwath equation:

$$\langle u^3 \rangle = \frac{\lambda \nu^2}{D B^2} \langle \frac{1}{\nu_t} \rangle + \frac{2\lambda}{D k^2} \langle \frac{u^2}{\nu_t} \rangle. \quad (37)$$

As in the Lagrangian case, this means that skewness (related to non-zero $\langle u^3 \rangle$) is generated through non-zero value of λ , i.e. through correlations of the multiplicative and the additive noise. However, due to the turbulent viscosity, we cannot explicitly solve the hierarchy of equation. In many homogeneous turbulent flows, however, the skewness (proportional to λ) is quite small, and moment of order $2n + 1$ are generally negligible in front of moments of order $2n + 2$. For even moments, this remark suggest that to first order in the skewness, and for $2n > 1$ the dynamics is simply given by:

$$\begin{aligned} k \partial_k \langle u^{2n} \rangle &= -\zeta(2n) \langle u^{2n} \rangle + 2n D B^2 k^2 \langle u^{2n+2} \rangle \\ &+ \alpha 2n (2n - 1) \langle u^{2n-2} \rangle + O(\lambda^2). \end{aligned} \quad (38)$$

Note that D/α is given by the parameter m_4 in our fit, and is such that Dk^2/α increases with k (see Figs. 26 and 27). Therefore, at small scales,

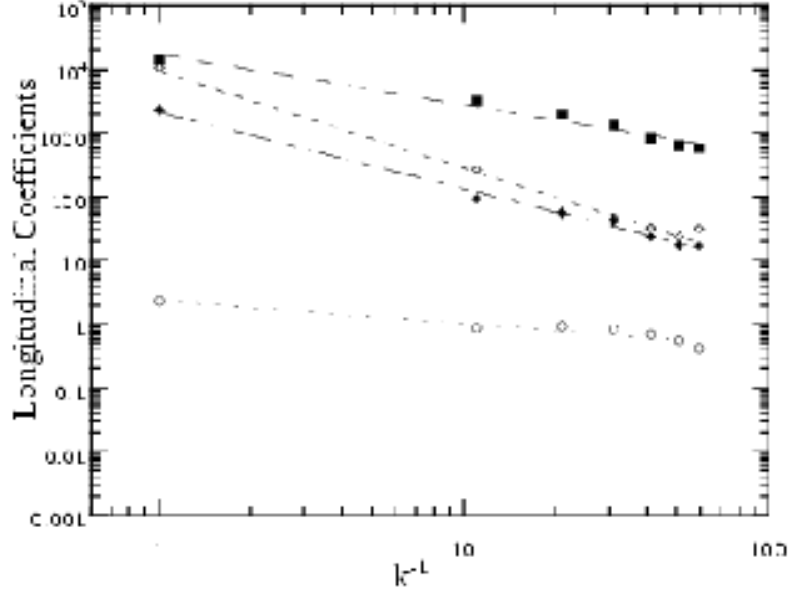


Figure 26: Coefficient of the fit of $d \ln(P)/du$ with (32) as a function of $1/k$ for longitudinal velocity increments: m_1 (squares), m_2 (empty diamonds), m_3 (circles) and m_4 (filled diamonds). The lines are the power-law fits: $k^{-0.79}$ (long-dashed line); $k^{-1.52}$ (short-dashed line); $k^{-0.36}$ (dotted line) and $k^{-1.2}$ (dash-dot line).

the dominant balance is:

$$k \partial_k \langle u^{2n} \rangle = 2nDB^2 k^2 \langle u^{2n+2} \rangle. \quad (39)$$

The solution is $\langle u^{2n} \rangle \propto k^{-2n}$. This is the usual "regular" scaling in the dissipative zone. For larger scales, $DB^2 k^2 \ll \alpha$, and if α varies like a power law, the general solution of (38) is a sum of power-laws:

$$\langle u^{2n} \rangle = \sum_{p=0}^n a_p \alpha^{n-p} k^{-\zeta(2p)}. \quad (40)$$

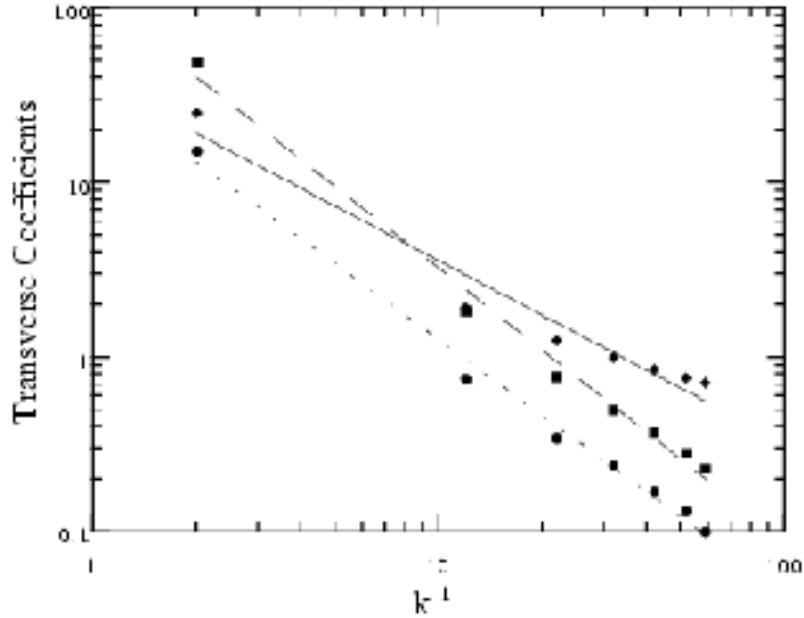


Figure 27: Coefficient of the fit of $d\ln(P)/du$ with (32) as a function of $1/k$ for transverse velocity increments: m_1 (squares), m_2 (diamonds), and m_4 (circles). The lines are the power-law fits: $k^{-1.56}$ (long-dashed line); $k^{-1.04}$ (line); and $k^{-1.45}$ (dotted line).

This solution illustrates the famous mechanism of "zero-mode intermittency" [22]. Here, the zero mode is the solution of the homogeneous part of eq. (38), i.e. a power-law of exponent $-\zeta(2n)$. Without the zeroth mode, responsible for the first $n - 1$ scaling laws, the $2n$ -th moment will scale in general like $\alpha(k)^n$ (provided one assume that this dominates the other term), i.e. will be related to the turbulent forcing. This is the standard Kolmogorov picture. When the zeroth mode is taken into account, the moment now includes new power laws, whose exponent is independent of the external forcing, and which can be dominant in the inertial range, thereby causing anomalous scaling. In the present case, the scaling exponent is quadratic in n , and reflects the log-normal statistics induced by the Gaussian multiplicative noise, in agreement with the latest wavelet analysis of Arneodo et al [4]. Note also that the

competition between the zeroth mode scaling and the scaling due to external forcing forbids the moments to scale like a power-law, thereby generating a breaking of the scale symmetry.

For *odd* moments, we cannot perform any rigorous expansion because all the terms of the equation are of order λ . For low order moments, however, the computation of $\langle u^{n+1}/\nu_t \rangle$ mainly involve velocity increments close to the center of the distribution, for which $\nu_t \approx \nu_0$. So, for low order, it is tempting to approximate the equation for the odd-order moments by

$$k\partial_k \langle u^{2n+1} \rangle \approx -\zeta(2n+1) \langle u^{2n+1} \rangle - 2n^2 \lambda B^2 \langle u^{2n+2} \rangle \nu^{-1}. \quad (41)$$

This approximation is only valid in the inertial range, where the last term of (36) can be neglected. An immediate consequence of this loose approximation is that $\zeta(2n+1) = \zeta(2n+2)$ in the inertial range. Odd moments (without absolute values) are very difficult to measure because of cancelation effects which introduce a lot of noise. In our case, due to our limited inertial range, we cannot compute these exponent with a sufficient degree of accuracy. A careful investigation performed in a high Reynolds number boundary layer [45] however seem to be in agreement with our prediction, as is shown in Fig. 28: it is striking to observe that $\zeta(5) \approx \zeta(6)$, $\zeta(7) \approx \zeta(8)$, etc making the curve look as if odd and even scaling exponents are organized on a separate curve [54]. A second independent experimental check of our prediction (41) is that $(\zeta(2n+2) - \zeta(2n+1)) \langle u^{2n+1} \rangle / \langle u^{2n+2} \rangle$ should scale, for $n > 3$ like n^2 . Fig. 29 shows that this is indeed the case.

3 Discussion

In this paper, we have shown that non-local interaction are responsible for intermittency corrections in the statistical behavior of 3D turbulence. Removal of the local interaction in numerical simulations leads to a substantial increase in the number of the tornado-like intense vortex filaments and to a stronger anomalous corrections in the higher cumulants of the velocity increments. It is also accompanied by a modification of the energy transfer in the inertial range, tending to create a flatter energy spectrum. The intermittency corrections and the spectra are close to that observed in high Reynolds number boundary layer, suggesting that the non-local interactions prevail in this geometry. This could be explained by presence of the mean

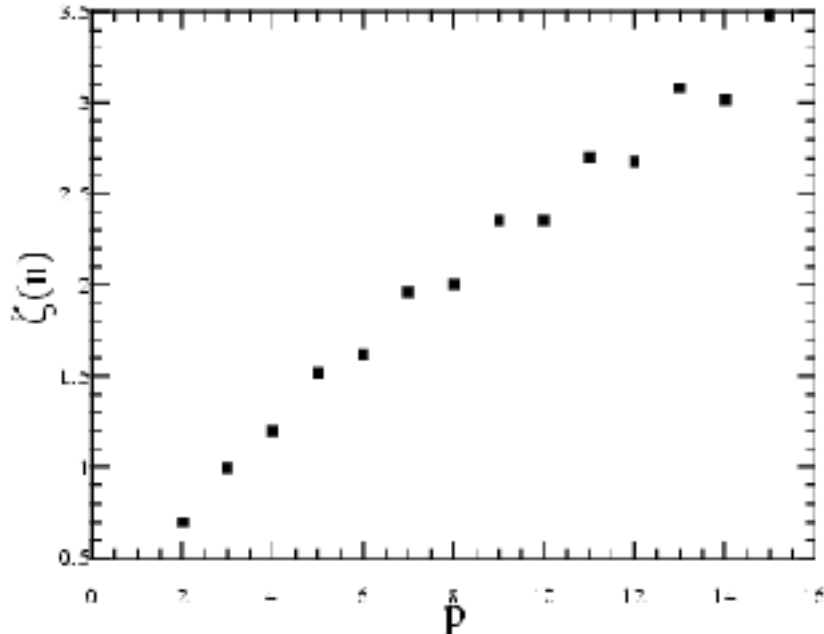


Figure 28: Exponents of the structure function in a high Reynolds number boundary layer [12]. Note the tendency for $\zeta(2n + 1) = \zeta(2n + 2)$ for $n > 3$.

flow, which geometrically favors non-local triads in the Fourier transform of the non-linear interactions. We showed that replacing the removed local interactions by a simple turbulent viscosity term allows to restore the correct intermittency and the energy characteristics. Our results agree with the belief that intermittency is related to thin vortices amplified by the external large scale strain similarly to the classical Burgers vortex solution. Local interactions can be viewed at mutual interaction of these thin intense vortices which result in their destruction, which is also in agreement with our results.

To prove that the enhanced intermittency is not simply the result of the stronger small-scale observed in the RDT simulation, we performed yet another numerical experiment in which the non-local interactions were neglected and only the local ones retained. This resulted in even higher (than in RDT) level of the small scales but it exhibited much less intermittency, which confirms our view that non-locality is crucial for generation of the

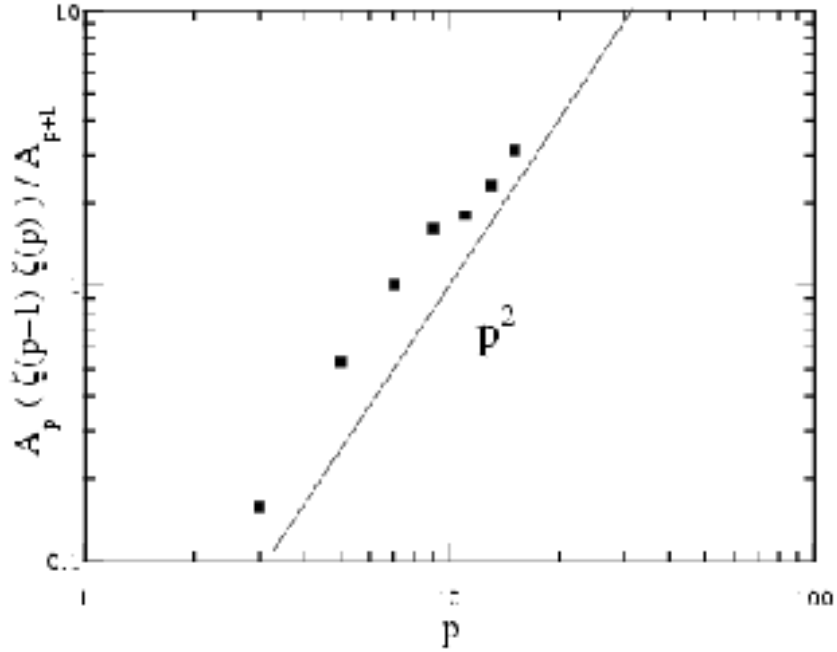


Figure 29: $(\zeta(2n + 2) - \zeta(2n + 1))A_{2n+1}/A_{2n+2}$ as a function of n in a high Reynolds number boundary layer. Here A_n is the prefactor of the (non-dimensional) structure function of order n . The line is n^2 , the prediction of our toy model.

intermittent structures.

The result that the net effect of the local interactions is to destroy the intermittent structures is at odds with a very common belief that the intermittency is due to the vortex reconnection process which takes a form of a finite time vorticity blow-up. Indeed, the later is a strongly nonlinear process in which the local vortex-vortex interactions are important. However, this process seems to be dominated by another local processes the net result of which is to destroy the high-vorticity structures rather than to create them. It would be premature to claim, however, that the same is true at any arbitrarily high Reynolds number.

Our numerical approach sets severe limitations to the value of the Reynolds number we are able to explore. In this context, it is interesting to point out that preliminary tests regarding the importance of non-local interactions have been conducted on a velocity field coming from a very large Reynolds number boundary layer [10]. Even though the test is not complete (the probes only permit the accurate measurement of special components of the velocity field), it tends to suggest that non-local interactions dominate the local interactions by several orders of magnitude. Our results would also explain the findings of the Lyon team [42], who found that when probing fluid area closer and closer to a large external vortices, or to a wall boundary, one could measure energy spectra moving from a $k^{-5/3}$ law towards a k^{-1} spectra, while anomalous corrections in scaling exponents would become more pronounced. At the light of our study, this could be simply explained by a trend towards more non-local dynamics via the mean-shear effects at the wall.

Based on the conclusions of our numerical study, we developed a new toy model of turbulence to study the intermittency. It has the form of a Langevin equation for the velocity increments with coupled multiplicative and additive noise. We showed how this toy model could be used to understand qualitatively certain observed features of intermittency and anomalous scaling laws. Among other things, we showed how the coupling between the two forces is related to the skewness of the distribution, and how algebraic and stretched exponential naturally arise from the competition between the multiplicative and the additive noise. We tested our qualitative predictions with experimental and numerical data, and found good general agreement. To be able to turn our toy model into a tool for "quantitative" study of the intermittency, several developments are needed. The first one is to consider the multi-dimensional version of our toy model, to be able to couple longitudinal and transverse increments. The scale dependence of the turbulent viscosity and of the forcing needs to be further investigated, possibly using tools borrowed from the Renormalization Group theory (see e.g. [9]). Also, the non-Gaussianity of the noises could be taken into account.

In 1994, Kraichnan [28] proposed an analytically solvable, new toy model for the passive scalar, which provided a substantial increase of our understanding of the passive scalar intermittency. Our model, built using the non-local hypothesis, is a direct heir of this philosophy in that, as in passive scalars, all important intermittency effects are produced via a linear dynamics. The nonlinear (local) scale interactions are important too because they

are the main carrier of the energy cascade, but it is only their mean effect and not statistical details that are essential.

the present paper.

Acknowledgments

BD acknowledges the support of a NATO fellowship and J-P Laval is thankful for the support of the *Laboratoire de Mécanique de Lille*, France. SN acknowledges the support of the TMR European network grant “Intermittency in Turbulent Systems” (ERB FMR XCT 98-0175). SN thanks Bob Kerr for useful discussion of the turbulent viscosity models. We thank Keith Moffatt, Oleg Zaboronki and our referees for suggesting an additional “local” numerical test which significantly reinforced our results.

References

- [1] B. Andreotti. *Action et réaction entre étirement et rotation, du laminaire au turbulent*. PhD thesis, Université de Paris 7, 1997.
- [2] B. Andreotti. Studying burger’s model to investigate the physical meaning of the alignments statistically observed in turbulence. *Phys. Fluids*, 9:735–742, 1997.
- [3] A. Arneodo, C. Baudet, F. Belin, R. Benzi, B. Castain, B. Chabaud, R. Chavarria, S. Ciliberto, R. Camussi, and F. Chilla. structure functions in turbulence in various flow configuration at Reynolds number between 30 and 5000 using extended self-similarity. *Europhys. Lett.*, 34:411–416, 1996.
- [4] A. Arneodo, S. Maneville, J. F. Muzy, and S. G. Roux. Revealing a log-normal cascading process in turbulent velocity statistics with wavelet analysis. *Philosophical Transaction of the Royal Society of London Series A-Mathematical Physical and Engineering Science*, 357:2415–2438, 1999.

- [5] R. Benzi, S. Ciliberto, R. Tripiccone, F Baudet, F. Massaioli, and S. Succi. Extended self similarity in turbulent flows. *Phys. Rev. E*, 48:R29, 1993.
- [6] V. Borue. Spectral exponents of entropy cascade in stationary homogeneous two dimensional turbulence. *Phys. Rev. Lett.*, 71:3967, 1994.
- [7] J. G. Brasseur and C. H. Wei. Interscale dynamics and local isotropy in high reynolds number turbulence within triadic interactions. *Phys. Fluids*, 6:842, 1994.
- [8] R. Camussi and R. Benzi. Hierarchy of transvers structure functions. *Phys. Fluids*, 9:257–259, 1997.
- [9] V. M. Canuto and Dubovikov. A dynamical model for turbulence. i. general formalism. *Phys. Fluids*, 8:571–586, 1996.
- [10] J. Carlier, J.-P. Laval, J. M. Foucaut, and M. Stanislas. Non-locality of the interaction of scales in high reynolds number turbulent boundary layer. *CRAS Série IIb*, 329:1–6, 2001.
- [11] B. Castaing. Consequences of an extremum principle in turbulence. *Journal de Physique*, 50:147, 1989.
- [12] B. Dhruva, Y. Tsuji, and K. R. Sreenivasan. Transverse structure functions in high-Reynolds-number turbulence. *Phys. Rev. E*, 56:R4928–R4930, 1997.
- [13] J. A. Domaradzki, W. Liu, C Härtel, and L. Kleiser. Energy transfer in numerically simulated wall-bounded turbulent flows. *Phys. Fluids*, 6:1583–1599, 1994.
- [14] Th Dombre. Private communication. 2000.
- [15] B. Dubrulle. Complex scaling laws and application. *submitted to European Phys. J.*, 1998.
- [16] B. Dubrulle. Affine turbulence. *Eur. phys. J. B*, 13:1, 2000.
- [17] B. Dubrulle. Finite size scale invariance. *Eur. phys. J. B*, 14:757–771, 2000.

- [18] B. Dubrulle and U. Frisch. Eddy viscosity of parity-invariant flow. *Phys. Rev. A*, 43:5355–5364, 1991.
- [19] R. Friedrich. At a turbulence in Dersden, in august 1998, R. Friedrich however suggested the possibility of two interacting multiplicative and additive noise in his presentation (unpublished). 1998.
- [20] R. Friedrich and Peinke. J. Description of a turbulent cascade by a Fokker-Planck equation. *Phys. Rev. Lett.*, 78:863, 1997.
- [21] U. Frisch. *Turbulence : The legacy of A.N. Kolmogorov*. Cambridge Univ. Press, 1995.
- [22] K Gawedski and A. Kupianen. Anomalous scaling of passive scalar. *Phys. Rev. Lett.*, 75:3834–3838, 1995.
- [23] E. B. Gledzer. *Sov. Phys. Dokl.*, 18:216, 1973.
- [24] J. Jimenez. Algebraic probability density tails in decaying isotropic two-dimensional turbulence. *J. Fluid Mech.*, 313:223–240, 1996.
- [25] A. N. Kolmogorov. The local structure of turbulence in incompressible viscous fluid for very large Reynolds number. *C.R. Acad. Sci URSS*, 30:301–305, 1941.
- [26] A. N. Kolmogorov. A refinement of previous hypotheses concerning the local structure of turbulence in a viscous incompressible fluid at high Reynolds number. *J. Fluid Mech.*, 13:82–85, 1962.
- [27] R. H. Kraichnan. Eddy viscosity in two and three-dimensions. *J. Atmosph. Science.*, 33:1521, 1976.
- [28] R. H. Kraichnan. Anomalous scaling of a randomly advected passive scalar. *Phys. Rev. Lett.*, 72:1016–1019, 1994.
- [29] J.-P. Laval and B Dubrulle. Numerical validation of a dynamical turbulent model of turbulence. *submitted to Phys. Rev. Lett.*, 2000.
- [30] J.-P. Laval, B. Dubrulle, and S. Nazarenko. Nonlocality of interaction of scales in the dynamics of 2D incompressible fluids. *Phys. Rev. Lett.*, 83:4061–4064, 1999.

- [31] J.-P. Laval, B. Dubrulle, and S. Nazarenko. Dynamical modeling of sub-grid scales in 2D turbulence. *Physica D: Nonlinear Phenomena*, 142:231–253, 2000.
- [32] P. Marcq and A. Naert. A langevin equation for turbulent velocity increments. *submitted to Phys. Fluids*, 2000.
- [33] Ph. Marcq and A. Naert. A Langevin equation for the energy cascade in fully-developped turbulence. *Physica D*, 124:368, 1998.
- [34] I. A. Min, I. Mezić, and A. Leonard. Lévy stable distribution for velocity and velocity difference in systems of vortex elements. *Phys. Fluids*, 8:1169–1180, 1996.
- [35] H. Nakao. Asymptotic power law of moments in a random multiplicative process with weak additive noise. *Phys. Rev. E*, 48:1691–1600, 1998.
- [36] S. Nazarenko. Exact solutions for near-wall turbulence theory. *Phys. Lett. A*, 264:444–448, 2000.
- [37] S. Nazarenko, N. K.-R. Kevlahan, and B. Dubrulle. WKB theory for rapid distortion of inhomogeneous turbulence. *J. Fluid Mech.*, 390:325–348, 1999.
- [38] S. Nazarenko, N. K.-R. Kevlahan, and B. Dubrulle. Nonlinear RDT theory of near-wall turbulence. *Physica D*, 139:158–176, 2000.
- [39] S. Nazarenko and J.-P. Laval. Non-local 2D turbulence and Batchelor’s regime for passive scalars. *J. Fluid Mech.*, 408:301–321, 2000.
- [40] G. Parisi and U. Frisch. On the singularity structure of fully developed turbulence. In M. Ghil, R. Benzi, and G. Parisi, editors, *Turbulence and Predictability in Geophysical Fluid Dynamics, Proceed. Inter. School of Physic ‘E. Fermi’, 1983, Varenna, Italy*. North-Holland, Amsterdam, 1985.
- [41] A. E. Perry, S. Henbest, and M. S. Chong. A theoretical and experimental study of wall turbulence. *J. Fluid Mech.*, 165:163–199, 1986.

- [42] J. F. Pinton, F. Chillà, and N. Mordant. Intermittency in the closed flow between coaxial corotating disks. *Eur. J. Mech. B/Fluids*, 17:535–547, 1998.
- [43] Z. S. She, E. Jakson, and Orszag S. A. Intermittent vortex structures in homogenous isotropic turbulence. *Nature*, 344:226, 1990.
- [44] E. D. Siggia. Numerical study of small-scale intermittency in 3-dimensional turbulence. *J. Fluid Mech.*, 107:375–406, 1981.
- [45] G. Stolovidsky, K. R. Sreenivasan, and A. Juneja. Scaling functions and scaling exponents in turbulence. *Phys. Rev. E.*, 48:R3217–R3220, 1993.
- [46] F Toschi, G. Amati, S. Succi, and R. Piva. Intermittency and structure functions in channel flow turbulence. *Phys. Rev. Lett.*, 82:5044–5047, 1999.
- [47] A. A. Townsend. *The structure of turbulent shear flow (second edition)*. Cambridge university press, Cambridge, 1976.
- [48] A. Tsinober, E. Kit, and T. Dracos. Experimental investigation of the field of velocity gradients in turbulent flows. *J. Fluid Mech.*, 82:169–192, 1992.
- [49] A. Vincent and M. Meneguzzi. The spatial structure and statistical properties of homogenous turbulence. *J. Fluid Mech.*, 225:1–20, 1991.
- [50] A. Vincent and M. Meneguzzi. The dynamics of vorticity tubes in homogenous turbulence. *J. Fluid Mech.*, 258:245–254, 1994.
- [51] V. Yakhot and S. A. Orzag. Renormalisation group analysis of turbulence. I. basic theory. *J. Sci. Comp.*, 1:3–51, 1986.
- [52] M. Yamada and K. Ohkitani. Lyapunov spectrum of a model of two-dimensional turbulence. *Phys. Rev. Lett.*, 60:983–986, 1988.
- [53] M. Yamada and K. Ohkitani. Temporal intermittency in the energy cascade process and local Lyapunov analysis in fully-developed turbulence. *Prog. Theor. Phys.*, 81:329–341, 1989.
- [54] L. Zubair. PhD thesis, Yale University, 1993.